AED: Adaptable Error Detection for Few-shot Imitation Policy

Jia-Fong Yeh 1 Kuo-Han Hung $^{*\,1}$ Pang-Chi Lo $^{*\,1}$ Chi-Ming Chung 2 Tsung-Han Wu 3 Hung-Ting Su 1 Yi-Ting Chen 4 Winston H. Hsu $^{1\,5}$

Abstract

We study how to report few-shot imitation (FSI) policies' behavior errors in novel environments, a novel task named adaptable error detection (AED). The potential to cause serious damage to surrounding areas limits the application of FSI policies in real-world scenarios. Thus, a robust system is necessary to notify operators when FSI policies are inconsistent with the intent of demonstrations. We develop a cross-domain benchmark for the challenging AED task, consisting of 329 base and 158 novel environments. This task introduces three challenges, including (1) detecting behavior errors in novel environments, (2) behavior errors occurring without revealing notable changes, and (3) lacking complete temporal information of the rollout due to the necessity of online detection. To address these challenges, we propose Pattern Observer (PrObe) to parse discernible patterns in the policy feature representations of normal or error states, whose effectiveness is verified in the proposed benchmark. Through our comprehensive evaluation, PrObe consistently surpasses strong baselines and demonstrates a robust capability to identify errors arising from a wide range of FSI policies. Moreover, we conduct comprehensive ablations and experiments (error correction, demonstration quality, etc.) to validate the practicality of our proposed task and methodology.

1. Introduction

Few-shot imitation (FSI), a framework that learns a policy in novel (unseen) environments from a few demonstrations, has recently drawn significant attention in the community (Dance et al., 2021; Hakhamaneshi et al., 2022; Tao et al., 2023; Shin et al., 2023; Liu et al., 2023b; Jiang et al., 2023). Notably, the framework, as exemplified by

(Duan et al., 2017; James et al., 2018; Bonardi et al., 2020; Dasari & Gupta, 2020; Dance et al., 2021; Yeh et al., 2022; Hakhamaneshi et al., 2022), has demonstrated its efficacy across a range of robotic manipulation tasks. This framework shows significant potential to adapt to a new task based on just a few demonstrations from their owners (Dance et al., 2021; Hakhamaneshi et al., 2022). However, a major barrier that still limits their ability to infiltrate our everyday lives is the ability to detect behavior errors in novel environments.

We propose a challenging and crucial task called adaptable error detection (AED), aiming to monitor FSI policies and report their behavior errors, and the corresponding benchmark. In this work, behavior errors refer to states that deviate from the demonstrated behavior, necessitating the timely termination of the policy upon their occurrence. Unlike existing few-shot visual perception tasks (Song et al., 2023), the failure can result in significant disruptions to surrounding objects and humans in the real world. Due to this nature, this often restricts real-world experiments to simple tasks. The AED benchmark we propose is built within Coppeliasim (Robotics) and Pyrep (James et al., 2019), encompassing six indoor tasks and one factory task. This comprehensive benchmark comprises 329 base environments and 158 new environments, spanning diverse domains and incorporating multiple stages. We aim to create a thorough evaluation platform for AED methodologies, ensuring their effectiveness before real-world deployment.

The AED tasks present three novel challenges, illustrated in Figure 1. First, AED entails monitoring a policy's behavior in novel environments, the normal states of which are not observed during training. Second, detecting behavior errors becomes challenging, as there are no noticeable changes to indicate when such errors occur. Specifically, this makes it difficult to discern either minor visual differences or misunderstandings of the task through adjacent frames. Third, AED requires online detection to terminate the policy timely, lacking complete temporal information of the rollout.

Current approaches struggle to address the unique challenges posed by AED. One-class classification (OCC) methods, including one-class SVMs (Zhou & Paffenroth, 2017) or autoencoders (Ruff et al., 2018; Park et al., 2018; Chen et al., 2020; Wong et al., 2021), face difficulties in handling

^{*}Equal contribution ¹National Taiwan University ²MediaTek Research ³University of California, Berkeley ⁴National Yang Ming Chiao Tung University ⁵ MobileDrive . Under review. <>

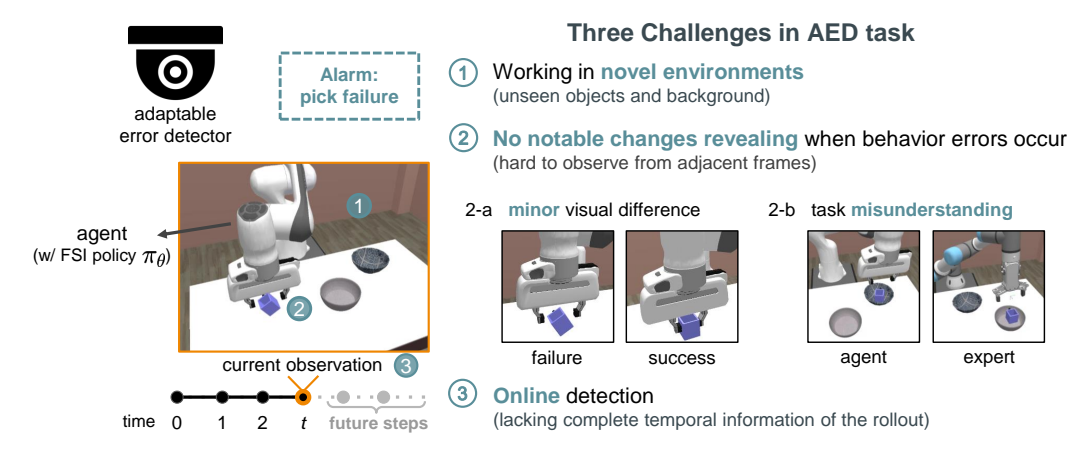


Figure 1. Our novel adaptable error detection (AED) task. To monitor the behavior of the few-shot imitation (FSI) policy π_{θ} , the adaptable error detector needs to address three challenges: (1) it works in novel environments, (2) no notable changes reveal when behavior errors occur, and (3) it requires online detection. These challenges make existing error detection methods infeasible.

unseen environments. These methods are trained solely with normal samples and identify anomalies by evaluating their significant deviation from the learned distribution. However, normal states in novel environments, which include unseen backgrounds and objects, are already considered out-of-distribution for these techniques, resulting in subpar performance. Multiple instance learning (Maron & Lozano-Pérez, 1997) or patch-based methods (Sultani et al., 2018; Roth et al., 2022) may alleviate the second challenge, particularly minor visual differences, in seen environments. However, the feasibility of applying these methods to AED remains underexplored. Video few-shot anomaly detection (vFSAD) methods (Sultani et al., 2018; Feng et al., 2021; Doshi & Yilmaz, 2023) are unsuitable for AED due to their dependency on full temporal observation from videos.

To this end, we introduce Pattern Observer (PrObe), a novel algorithm that extracts discriminative features from the monitored policy to identify instances of behavior errors. Specifically, PrObe designs a gating mechanism to extract task-relevant features from the monitored FSI policy to mitigate the impact of a novel environment. Then, we design an effective loss function to distill sparse pattern features, making it easier to observe changes in observation. Additionally, we design a recurrent generator to generate a pattern flow of current policy. Finally, we determine if there is a behavior error by proposing a novel temporal-aware contrastive objective to compare the pattern flow and demonstrations.

We conduct thorough experiments on the proposed benchmark. PrObe outperforms several strong baselines, demonstrating a significant performance boost of up to 40%. We also demonstrate PrObe is robust to different FSI policies. Next, we conduct a thorough ablative study to justify the effectiveness of our design choice. Furthermore, we report covering timing accuracy, embedding visualization, error correction, and demonstration quality to validate our claims and the practicality of our task and method.

Contributions We make three significant contributions in this study: (1) We define a vital yet underexplored task called adaptable error detection (AED). (2) We introduce a novel benchmark and present PrObe, facilitating the research community to delve into this important area collectively. (3) We conduct thorough evaluations on our proposed benchmark, demonstrating the effectiveness of PrObe. It surpasses several baseline models and exhibits robustness across different policies. Our research is anticipated to serve as a key foundation for future real-world experiments in the field of FSI research.

2. Related Works

2.1. Few-shot Imitation (FSI)

Policy With the recent progress in meta-learning (Finn et al., 2017a), the community explores the paradigm for learning policies from limited demonstrations during inference (Finn et al., 2017b; Yu et al., 2018; 2019a). Notably, these works either assume that the agent and expert have the same configuration or explicitly learn a motion mapping between them (Yu et al., 2018). Conversely, DC methods (Dance et al., 2021; Yeh et al., 2022; Watahiki & Tsuruoka, 2022) develop a policy that behaves conditioned both on the current state and demonstrations. Furthermore, they implicitly learn the mapping between agents and experts, making fine-tuning optional. Thereby, effectively extracting knowledge from demonstrations becomes the most critical matter. In most FSI works, no environment interactions are allowed before inference. Hence, policies are usually trained by behavior cloning (BC) objectives, i.e., learning the likelihood of expert actions by giving expert observations. Recently, DCRL (Dance et al., 2021) trains a model using reinforcement learning (RL) objects and performs FSI tasks without interacting with novel environments.

Evaluation tasks Since humans can perform complex long-horizon tasks after watching a few demonstrations, FSI studies continuously pursue solving long-horizon tasks to verify if machines can achieve the same level. A set of research applies policy on a robot arm to perform daily life tasks in the real world (Yu et al., 2018) or simulation (Duan et al., 2017). The task is usually multi-stage and composed of primitives/skills/stages (Yeh et al., 2022; Hakhamaneshi et al., 2022), such as a typical pick-and-place task (Yu et al., 2019a) or multiple boxes stacking (Duan et al., 2017). Besides, MoMaRT (Wong et al., 2021) tackles a challenging mobile robot task in a kitchen scene.

Our work formulates the AED task for the safety concern of FSI policies and proposes PrObe to address it, which is valuable for extensive FSI research. Besides, we have also built challenging FSI tasks containing attributes such as scenes from different fields, realistic simulation, task distractors, and various robot behaviors

2.2. Few-shot Anomaly Detection (FSAD)

Problem setting Most existing FSAD studies deal with anomalies in images (Roth et al., 2022; Sheynin et al., 2021; Pang et al., 2021; Huang et al., 2022a; Wang et al., 2022) and only a few tackle anomalies in videos (Lu et al., 2020; Qiang et al., 2021; Huang et al., 2022b; Doshi & Yilmaz, 2023). Moreover, problem settings are diverse. Some works presume only normal data are given during training (Sheynin et al., 2021; Wang et al., 2022; Lu et al., 2020; Qiang et al., 2021), while others train models with normal and a few anomaly data and include unknown anomaly classes during inference (Pang et al., 2021; Huang et al., 2022b).

Method summary Studies that only use normal training samples usually develop a reconstruction-based model with auxiliary objectives, such as meta-learning (Lu et al., 2020), optical flow (Qiang et al., 2021), and adversarial training (Sheynin et al., 2021; Qiang et al., 2021). Besides, patch-based methods (Pang et al., 2021; Roth et al., 2022) reveal the performance superiority on main image FSAD benchmark (Bergmann et al., 2019) since the anomaly are tiny defeats. Regarding video few-shot anomaly detection (vFSAD), existing works access a complete video to compute the temporal information for determining if it contains anomalies. In addition, vFSAD benchmarks (Mahadevan et al., 2010; Lu et al., 2013) provide frame-level labels to evaluate the accuracy of locating anomalies in videos.

Comparison between vFSAD and AED task Although both the vFSAD and our AED task require methods to perform in unseen environments, there are differences: (1) The anomalies in vFSAD involve common objects, while AED methods monitor the policy's behavior errors. (2) An anomaly in vFSAD results in a notable change in the

perception field, such as a cyclist suddenly appearing on the sidewalk (Mahadevan et al., 2010). However, no notable change is evident when a behavior error occurs in AED. (3) The whole video is accessible in vFSAD (Sultani et al., 2018; Feng et al., 2021; Doshi & Yilmaz, 2023), allowing for the leverage of its statistical information. In contrast, AED requires online detection to terminate the policy timely, lacking the complete temporal information of the rollout. These differences make our AED task more challenging and also render vFSAD methods infeasible.

3. Preliminaries

Few-shot imitation (FSI) FSI is a framework worthy of attention, accelerating the development of human-robot collaboration, such as robots completing pre-tasks alone or interacting with humans for highly complex tasks. Following Yeh et al. (2022), a FSI task is associated with a set of base environments E^b and novel environments E^n . In each novel environment $e^n \in E^n$, a few demonstrations \mathcal{D}^n are given. The objective is to seek a policy π that achieves the best performance (e.g., success rate) in novel environments leveraging a few demonstrations. Notably, the task in base and novel environments are semantically similar, but their backgrounds and interactive objects are disjoint. Besides, observations and demonstrations are RGB-D images that only provide partial information, as seen in recent studies (Dasari & Gupta, 2020; Yeh et al., 2022). Besides, addressing FSI tasks typically involves three challenges in practice: (1) The task is multi-stage, (2) Demonstrations are lengthvariant and misaligned, and (3) The expert and agent have a distinct appearance or configuration, as presented in Yeh et al. (2022). Developing a policy to solve the FSI task and simultaneously tackle these challenges is crucial.

Demonstration-conditioned (**DC**) **policy** As stated above, the expert and agent usually have different appearances or configurations. The DC policy $\pi(a \mid s, \mathcal{D})$ learns implicit mapping using current states s and demonstrations \mathcal{D} to compute agent actions a. Next, we present the unified architecture of DC policies and how they produce the action. When the observations and demonstrations are RGB-D images that only provide partial information, we assume that current history h (observations from the beginning to the latest) and demonstrations are adopted as inputs.

A DC policy comprises a feature encoder, a task-embedding network, and an actor. After receiving the rollout history h, the feature encoder extracts the history features f_h . Meanwhile, the feature encoder also extracts the demonstration features. Then, the task-embedding network computes the task-embedding f_{ζ} to retrieve task guidance. Notably, the lengths of agent rollout and demonstrations can vary. The task-embedding network is expected to handle length-

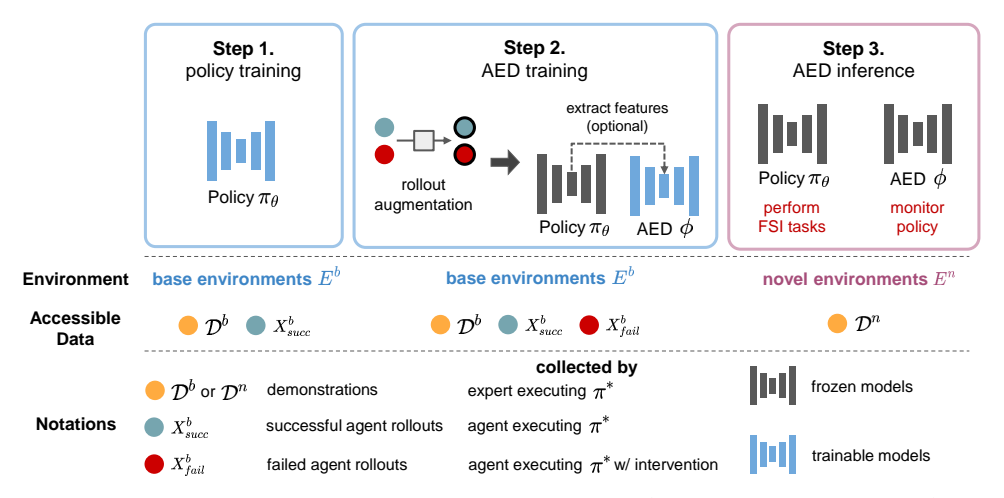


Figure 2. AED protocol. Before training, we collect successful agent rollouts X^b_{succ} , failed agent rollouts X^b_{fail} , and a few expert demonstrations \mathcal{D}^b for all base environments E^b . Then, the process contains three phases: policy training, AED training, and AED inference. The adaptable error detector ϕ aims to report policy π_{θ} 's behavior errors when performing in novel environments E^n .

variant sequences by padding frames to a prefixed length or applying attention mechanisms. Afterward, the actor predicts the action for the latest observation, conditioned on the history features f_h and task-embedding f_ζ . Additionally, an optional inverse dynamics module predicts the action between consecutive observations to improve the policy's understanding of how actions affect environmental changes. At last, the predicted actions are optimized by the negative log-likelihood or regression objectives (MSE).

4. AED task

Our AED task is formulated to monitor and report FSI policies' behavior errors, i.e., states of policy rollouts that are inconsistent with demonstrations. The challenges associated with this task have been presented in Section 1. Next, we formally state our novel AED task.

Problem statement Let c denote the category of agent's behavior status, where $c \in \mathbf{C}$, $\mathbf{C} = \{\text{normal, error}\}$. When the agent with the trained FSI policy π_{θ} performs in a novel environment e^n , an adaptable error detector ϕ can access the agent's rollout history h and few expert demonstrations \mathcal{D}^n . It then predicts the categorical probability \hat{y} of the behavior status for the latest state in the history h by

$$\hat{y} = \phi(h, \mathcal{D}^n) = P(c \mid enc(h, \mathcal{D}^n)), \tag{1}$$

where enc denotes the feature encoder, and it may be enc_{ϕ} (ϕ contains its own encoder) or $enc_{\pi_{\theta}}$ (based on policy's encoder). Next, let y represent the ground truth probability, we evaluate ϕ via the expectation of detection accuracy over agent rollouts X^n in all novel environments E^n :

$$\mathbb{E}_{e^n \sim E^n} \mathbb{E}_{e^n, \pi_{\theta}(\cdot|\cdot, \mathcal{D}^n)} \mathbb{E}_{h \sim X^n} A(\hat{y}, y), \tag{2}$$

where $A(\cdot, \cdot)$ is the accuracy function that returns 1 if \hat{y} is consistent with y and 0 otherwise. However, frame-level labels are lacking in novel environments since we only know if the rollout is successful or failed at the end. Hence, we present the details of $A(\cdot, \cdot)$ in the Appendix's Section E.1.

Protocol To train the detector ϕ , we assume it can access the resources in base environments E^b just like FSI policies, i.e., successful agent rollouts X_{succ}^{b} and a few expert demonstrations \mathcal{D}^b , which are collected by executing the agent's and expert's optimal policies π^{*1} , respectively. Besides, we collect failed agent rollouts X_{fail}^{b} by intervening in the agent's π^* at a critical timing (e.g., the moment to grasp objects) so that X^b_{fail} can possess precise frame-level error labels. Figure 2 shows the protocol: (1) Policy π_{θ} is optimized using successful agent rollouts X_{succ}^{b} and few demonstrations \mathcal{D}^b . (2) Detector ϕ is trained on agent rollouts X^b_{succ} , X^b_{fail} and few demonstrations \mathcal{D}^b . Besides, ϕ extracts features from policy π_{θ} if it depends on policy's encoder. And π_{θ} 's parameters are not updated in this duration. (3) No agent rollouts are pre-collected in novel environments E^n ; policy π_{θ} solves the task leveraging few demonstrations \mathcal{D}^n . And the detector ϕ monitors policy π_{θ} 's behavior during the progress. Our AED task aims to evaluate the detector ϕ 's ability to report policy π_{θ} 's behavior errors.

5. Pattern Observer (PrObe)

Overview Apart from formulating the AED task, we also develop a tailored method to address it. Our motivation is to detect behavior errors in the space of policy features to acquire additional task-related knowledge. Thus, an adapt-

¹The agent's optimal policy is expected to be known during training. Besides, successful agent rollouts are not expert demonstrations since the agent and expert have different configurations.

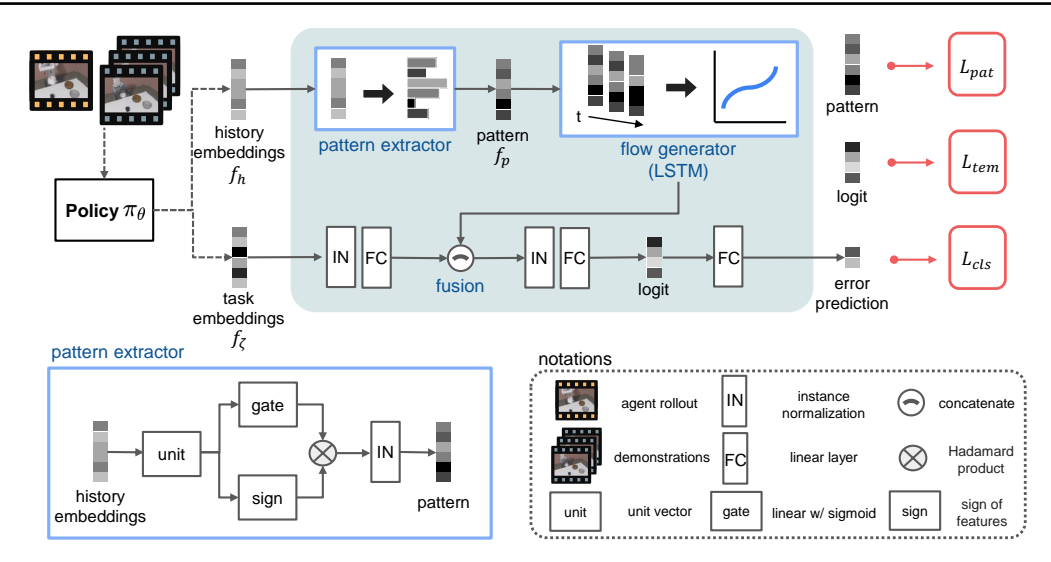


Figure 3. Architecture of PrObe. PrObe detects behavior errors through the pattern extracted from policy features. The learnable gated pattern extractor and flow generator (LSTM) compute the pattern flow of history features f_h . Then, the fusion with transformed task-embeddings f_{ζ} aims to compare the task consistency. PrObe predicts the behavior error based on the fused embeddings. Objectives, L_{pat} , L_{tem} , and L_{cls} , optimize the corresponding outputs.

able error detector, Pattern Observer (PrObe), is proposed to discover the unexpressed patterns in the policy features extracted from frames of successful or failed states. Even if the visual inputs vary during inference, PrObe leverages the pattern flow and a consistency comparison to alleviate the challenges shown in Figure 1. As a result, it can address the AED task effectively. Furthermore, a rollout augmentation is designed to increase rollout diversity and enhance the method's robustness, as we now present in detail.

5.1. Rollout Augmentation

To obtain rollouts with balanced outcomes (successful or failed) and precise frame-level labels, we collect X^b_{succ} and X^b_{fail} using the agent's optimal policy π^* with intervention rather than the trained FSI policy π_{θ} . However, even if the policy π_{θ} is trained on X^b_{succ} (collected from the agent's optimal policy π^*), the trained π_{θ} will still deviate from agent's π^* due to the limited rollout diversity. In other words, a behavior bias exists between the two policies, which should be reduced. Otherwise, an adaptable error detector trained on original collected X^b_{succ} and X^b_{fail} will yield a high false-positive during AED inference.

Accordingly, we augment agent rollouts so as to increase rollout diversity and dilute the behavior bias between trained π_{θ} and agent's π^* . Specifically, we iterate each frame (and its label) from sampled agent rollouts and randomly apply the following operations: keep, drop, swap, and copy, with probability 0.3, 0.3, 0.2, and 0.2, respectively. As a result, we inject distinct behaviors into collected rollouts, such as speeding up (interval frames dropped), slowing down (repetitive frames), and not smooth movements (swapped frames). We carefully verify its benefits in Section 6.

5.2. PrObe Architecture

As depicted in Figure 3, PrObe comprises three major components: a pattern extractor, a pattern flow generator, and an embedding fusion. Since PrObe detects errors through policy features, the history features f_h and task-embeddings f_ζ from the trained policy π_θ are passed into PrObe.

At first, the pattern extractor aims to gather discriminative information from each embedding of history features f_h . In more detail, f_h is transformed into unit embeddings divided by its L2 norm, mitigating biases caused by changes in visual inputs. Then, a learnable gate composed of a linear layer with a sigmoid function determines the importance of each embedding cell. A Hadamard product between the sign of unit embeddings and the importance scores, followed by an instance normalization (IN), is applied to obtain the pattern features f_p for each timestep. PrObe then feeds f_p into a flow generator (a LSTM) to generate the pattern flow. Intuitively, the changes in the pattern flow of successful and failed rollouts will differ. On the other hand, the task-embeddings f_{ζ} are transformed by an IN layer, a linear layer (FC), and a tanh function. This step maps the task-embeddings into a space similar to the pattern flow. Then, a fusion process concatenates the pattern flow and transformed task-embeddings to compute the error predictions \hat{y} . This process compares the consistency between the agent rollout and demonstrations and uses this as a basis for determining whether behavior errors occur.

Objectives PrObe is optimized by one supervised and two unsupervised objectives. First, since accurate frame-level error labels y are available during training, a binary crossentropy (BCE) objective L_{cls} is used to optimize the error

prediction \hat{y} . Second, L_{pat} is an L1 loss applied to the pattern features f_p , which encourages the pattern extractor to generate sparse pattern features, making it easier to observe changes. In addition, a contrastive objective L_{tem} is added to logit embeddings (the embedding before the final outputs) to reinforce the difference between the normal and error states in failed rollouts X_{fail}^b , i.e., we sample anchors from X_{fail}^b , and the positive and negative samples will be logits of the same or opposed states from the same rollout.

However, the logits of adjacent frames will contain similar signals since they contain temporal information from the pattern flow, even if behavioral errors have occurred (cf. Appendix's Figure 7). Blindly forcing the logits of normal and error states to be far away from each other may mislead the model and have a negative impact. Hence, L_{tem} is a novel temporal-aware triplet loss (Schroff et al., 2015) calculated by:

$$L_{tem} = \frac{1}{N} \sum_{i=0}^{N} \max(\|\text{logit}_{i}^{a} - \text{logit}_{i}^{p}\|_{2} - \|\text{logit}_{i}^{a} - \text{logit}_{i}^{n}\|_{2} + m_{t}, 0),$$
(3)

where N is the number of sampled pairs, and the temporal-aware margin $m_t = m*(1.0 - \alpha*(d_{ap} - d_{an}))$ will be enlarged or reduced considering the temporal distance of anchor, positive and negative samples. Among them, m is the margin in the original triplet loss, and d_{ap} , d_{an} are the clipped temporal distances between the anchor and positive sample and the anchor and negative sample, respectively. Ultimately, the total loss L_{total} combines L_{pat} , L_{tem} , L_{cls} objectives weighted by λ_{pat} , λ_{tem} , and λ_{cls} .

6. Experiments

Our experiments aim to verify the following questions: (1) Is learning how to discern patterns in the space of policy features actually beneficial for addressing the AED task? (2) Is our proposed PrObe highly general, robust and interpretable? (3) Is the proposed AED task practical and helpful to the research community?

6.1. Experimental Settings

Evaluation tasks Existing robotic manipulation benchmarks (James et al., 2020; Fu et al., 2020; Li et al., 2022; Gu et al., 2023) do not suit our needs due to the novel challenges posed by the AED task. We design seven multi-stage FSI tasks (six indoor and one factory scene) that contain the challenges introduced in Section 3. Detailed task descriptions, schematic, the number of environments, and distractors are shown in the Appendix's Section D. We build the tasks on Coppeliasim software (Robotics) and use Pyrep (James et al., 2019) toolkit as a coding interface.

FSI policies To verify if the AED methods can handle various policies' behaviors, we select three representative DC policies to perform FSI tasks, which are implemented following the descriptions in Section 3 and use the same feature extractor and actor architecture. The main difference between them is how they extract task-embeddings from expert demonstrations. NaiveDC (James et al., 2018)² concatenates the first and last frames of demonstrations and averages their embeddings as task-embeddings; DCT (Dance et al., 2021)³ performs cross-demonstration attention and fuses them at the time dimension; SCAN (Yeh et al., 2022) computes the tasks-embeddings using stage-conscious attention to locate the critical frames in demonstrations.

Baselines PrObe is compared with four error detection methods that possess different characteristics. Unlike PrObe, all methods are policy-independent (i.e., containing their own encoders) and use the same encoder architecture. We provide the detailed baseline introduction in Section C of Appendix and briefly describe them below: (1) SVDDED, an one-class SVM modified from Ruff et al. (2018), is a single-frame DC method trained with only successful rollouts. (2) TaskEmbED, a single-frame DC method trained with successful and failed rollouts, uses the NaiveDC (James et al., 2018) policy's strategy to extract task-embeddings when predicting errors. (3) LSTMED is a LSTM model (Hochreiter & Schmidhuber, 1997) that predicts errors without demonstration information. (4) DCTED leverages the DCT (Dance et al., 2021) policy's strategy to predict errors.

Metrics The area under the receiver operating characteristic (AUROC) and the area under the precision-recall curve (AUPRC), two conventional threshold-independent metrics in error (or anomaly) detection literature, are reported. We linearly select 5000 thresholds spaced from 0 to 1 (or SVDDED's outputs) to compute the two scores. The accuracy function (cf. Appendix's Section E.1) determines the error prediction results (i.e., TP, TN, FP, FN) at the sequence-level so that we further conduct and illustrate the timing accuracy experiment in Figure 5.

6.2. Analysis of Experimental Results

Main experiment Our main experiment aims to answer the first two questions. We let three policies perform all seven FSI tasks and record their rollouts' observations and outcomes (success or failure). Then, AED methods infer the error predictions and report values on the two metrics (third stage in Figure 2). It is worth noting that policies behave differently, making it difficult for AED methods to effectively detect behavioral errors in all policies. Furthermore, in our experiments, AUPRC has more reference value

 $^{^2}$ TaskEmb \rightarrow NaiveDC, avoiding confusion w/ AED baselines.

 $^{^3}$ DCRL \rightarrow DCT (transformer), since we don't use RL training.

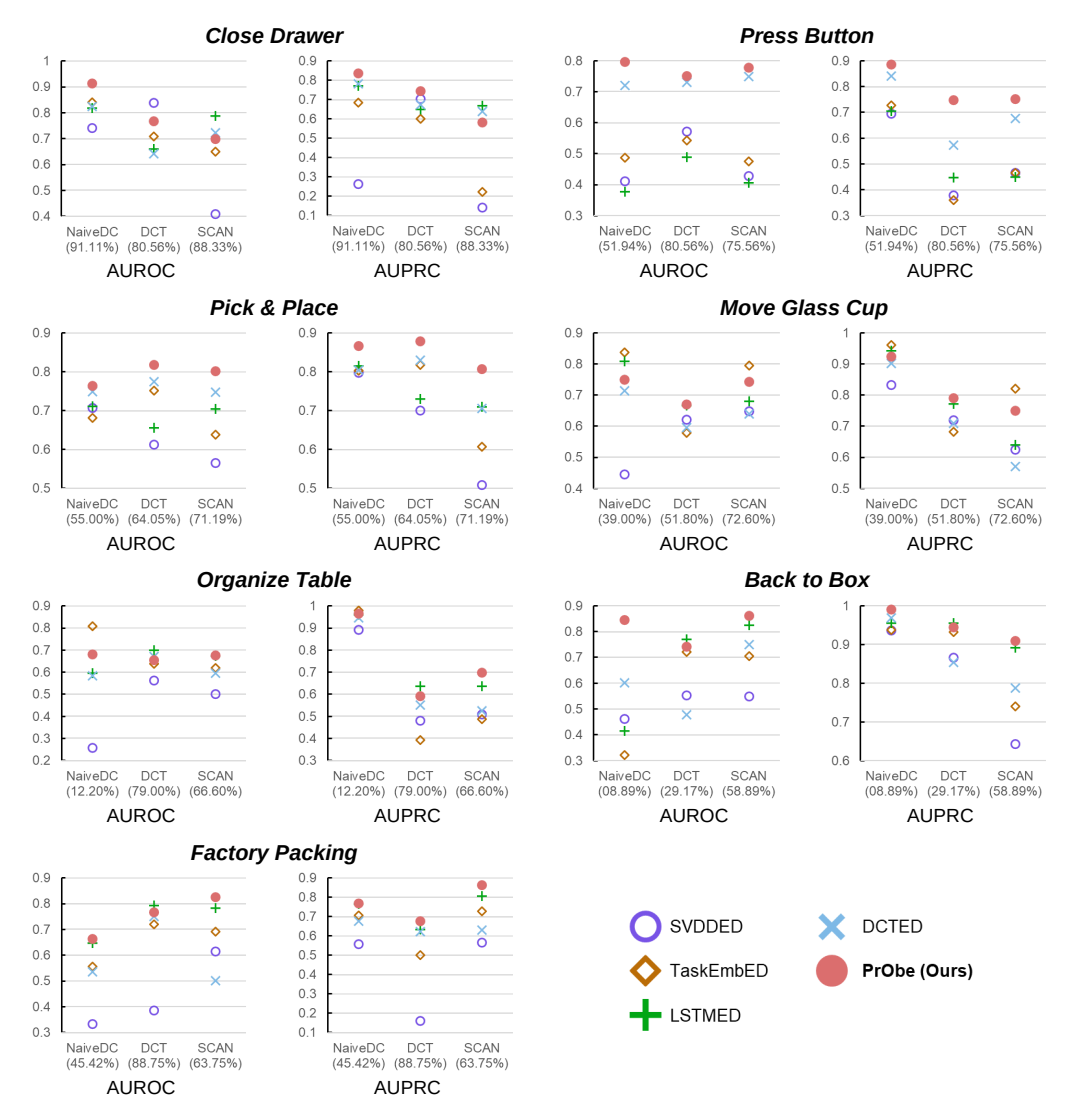


Figure 4. AED methods' performance on our seven challenging FSI tasks. The value under the policy indicates the policy's success rate in that task. The ranges of the two metrics [↑] are both 0 to 1. Our PrObe gets the best 13 AUROC and 15 AUPRC scores out of 21 cases (top of each column), demonstrating its superiority and robustness. We refer to the Appendix's Table 8 for detailed values.

because the results of policy rollout are often biased (e.g., many successes or failures), AUPRC is less affected by the class imbalance of outcomes.

From Figure 4, PrObe effectively reports the inconsistency between rollout frames and demonstrations (i.e., behavior errors) in novel environments, even identifying some errors not included in the training data. Specifically, it achieves the best 13 AUROC and 15 AUPRC results out of 21 cases, showcasing its superiority among AED methods and its robustness across different policies. Besides, we investigated the cases where PrObe exhibited suboptimal performance and found that they can be grouped into two types: (1) Errors all occur at the same timing (e.g., at the end of the rollout) and can be identified without reference to the demonstrations (e.g., DCT policy in *Organize Table* task). (2) Errors are not as obvious compared to the demonstra-

tions, and there is still a chance to complete the task, such as the drawer being closed to a small gap (SCAN and DCT policies in *Close Drawer* task). In these cases, the pattern flow will not change enough to be recognized, resulting in suboptimal results for PrObe.

Timing accuracy Our main experiment examines whether AED methods can accurately report behavior errors when receiving complete policy rollouts. To further verify if they identify errors at the right timing, we manually annotated a subset of rollouts (SCAN policy in *Pick & Place* task) and visualized the raw outputs of all AED methods. SVDDED outputs the embedding distance between observation and task-embedding, while others compute the probabilities, as shown in Figure 5. In the successful rollout case, both our PrObe and LSTMED stably recognize the states as normal,

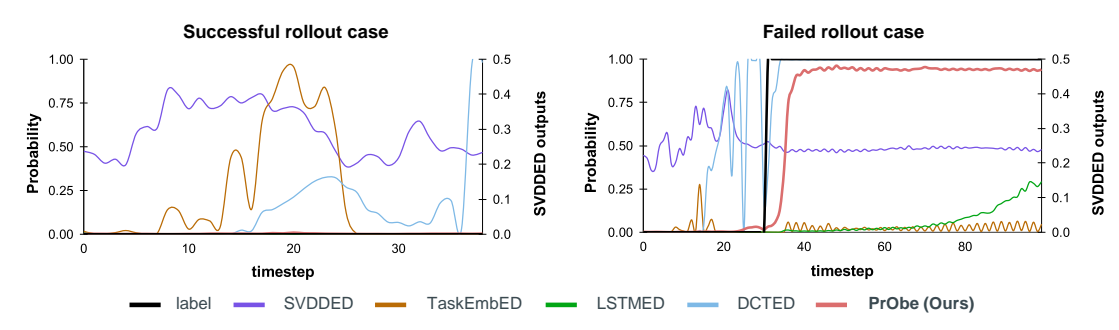


Figure 5. Visualization of timing accuracy. Raw probabilities and SVDDED outputs of selected successful (left) and failed (right) rollouts are drawn. PrObe raises the error at the accurate timing in the failed rollout and stably recognizes normal states in the successful case.

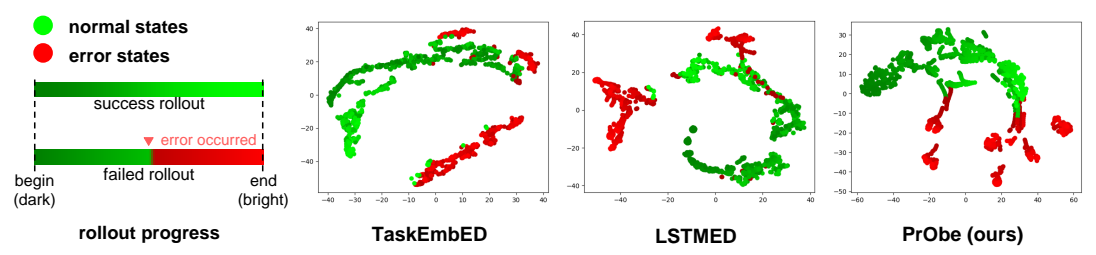


Figure 6. t-SNE visualization of learned embeddings (representations). The green and red circles represent normal and error states, respectively. The brightness of the circle indicates the rollout progress (from dark to bright). The embeddings learned by our PrObe have better interpretability because they exhibit task progress and homogeneous state clustering characteristics.

while other methods misidentify and increase the probability that inputs may be the error states. In the failed rollout case, PrObe detects the error after it has persisted for a while (< 5 frames) and significantly increases the probability. We attribute this short delay to the fact that the pattern flow takes a short period to cause enough change. Even so, PrObe is the one that detects the error at the closest timing; other methods raise the probability either too early or too late. We emphasize that this situation is ubiquitous and not a deliberate choice.

Embedding visualization To analyze whether the learned embeddings possess discernible patterns, we initially extract the same 20 rollouts from the annotated dataset above using three AED methods to obtain the embeddings. Subsequently, we present the t-SNE transform (van der Maaten & Hinton, 2008) on these embeddings in Figure 6. Obviously, the embeddings learned by TaskEmbED and LSTMED are scattered and lack an explainable structure. In contrast, our PrObe's embeddings exhibit characteristics of task progress and homogeneous state clustering, i.e., the states with similar properties (e.g., the beginnings of rollouts, the same type of failures) are closer. This experiment supports the hypothesis that PrObe can learn implicit patterns from the policy's feature embeddings.

Ablations and supportive experiments To further verify the second question, we conduct and summarize comprehensive ablations in the Appendix. First, Figure 11 indicates that the proposed rollout augmentation (RA) strategy can increase the rollout diversity and benefits AED methods

with temporal information. Second, Figure 12 proves that PrObe's design can effectively improve performance. Third, Figure 13 shows PrObe's performance stability by executing multiple experiment runs on a subset of tasks and computing the performance variance. Fourth, we examine how AED methods' performance is influenced when receiving demonstrations with distinct qualities, as presented in Table 6. Regarding the third question, we provide the pilot study's result on error correction in Table 7 to demonstrate the AED task's practicality. Please refer to the corresponding paragraphs in the Appendix for exhaustive versions.

7. Conclusion

We point out the importance of monitoring policy behavior errors to accelerate the development of FSI research. To this end, we formulate the novel adaptable error detection (AED) task, whose three challenges make previous error detection methods infeasible. To address AED, we propose the novel Pattern Observer (PrObe) by detecting errors in the space of policy features. With the extracted discernible patterns and additional task-related knowledge, PrObe effectively alleviates AED's challenges. It achieves the best performance, as confirmed by both our primary experiment and thorough ablation analyses. We also demonstrate PrObe's robustness in the timing accuracy experiment and the learned embedding visualization. Finally, we provide the pilot study on error correction to reveal the practicality of our AED task. Our work is an essential cornerstone in developing future FSI research to conduct complex real-world experiments.

Impact Statement

Our work aims to address a critical learning task (i.e., error detection of policy behaviors), accelerating the development of safety-aware robotic applications in real-world scenarios. We feel that our research will not have any potential negative impacts or ethical concerns for society.

References

- Anderson, G., Chaudhuri, S., and Dillig, I. Guiding safe exploration with weakest preconditions. In *The Eleventh International Conference on Learning Representations*, 2023. URL https://openreview.net/forum?id=zzqBoIFOQ1.
- Bergmann, P., Fauser, M., Sattlegger, D., and Steger, C. Mytec ad a comprehensive real-world dataset for unsupervised anomaly detection. In 2019 IEEE/CVF Conference on Computer Vision and Pattern Recognition (CVPR), pp. 9584–9592, 2019.
- Bonardi, A., James, S., and Davison, A. J. Learning one-shot imitation from humans without humans. *IEEE Robotics and Automation Letters*, 5(2):3533–3539, 2020.
- Chen, T., Liu, X., Xia, B., Wang, W., and Lai, Y. Unsupervised anomaly detection of industrial robots using sliding-window convolutional variational autoencoder. *IEEE Access*, 8:47072–47081, 2020.
- Cui, Y., Karamcheti, S., Palleti, R., Shivakumar, N., Liang, P., and Sadigh, D. No, to the right: Online language corrections for robotic manipulation via shared autonomy. In *Proceedings of the 2023 ACM/IEEE International Con*ference on Human-Robot Interaction, pp. 93–101, 2023.
- Dance, C. R., Perez, J., and Cachet, T. Demonstration-conditioned reinforcement learning for few-shot imitation. In *Proceedings of the 38th International Conference on Machine Learning*, volume 139, pp. 2376–2387, 18–24 Jul 2021.
- Dasari, S. and Gupta, A. Transformers for one-shot imitation learning. In *Proceedings of the Conference on Robot Learning*, 2020.
- Doshi, K. and Yilmaz, Y. Towards interpretable video anomaly detection. In 2023 IEEE/CVF Winter Conference on Applications of Computer Vision (WACV), pp. 2654–2663, 2023. doi: 10.1109/WACV56688.2023. 00268.
- Duan, Y., Andrychowicz, M., Stadie, B., Ho, J., Schneider, J., Sutskever, I., Abbeel, P., and Zaremba, W. One-shot imitation learning. In *Advances in Neural Information Processing Systems*, volume 30, 2017.

- Feng, J.-C., Hong, F.-T., and Zheng, W.-S. Mist: Multiple instance self-training framework for video anomaly detection. In 2021 IEEE/CVF Conference on Computer Vision and Pattern Recognition (CVPR), pp. 14004–14013, 2021
- Finn, C., Abbeel, P., and Levine, S. Model-agnostic metalearning for fast adaptation of deep networks. In *Proceedings of the 34th International Conference on Machine Learning*, volume 70 of *Proceedings of Machine Learning Research*, pp. 1126–1135, 06–11 Aug 2017a.
- Finn, C., Yu, T., Zhang, T., Abbeel, P., and Levine, S. One-shot visual imitation learning via meta-learning. In *CoRL* 2017, pp. 357–368, 13–15 Nov 2017b.
- Fu, J., Kumar, A., Nachum, O., Tucker, G., and Levine, S. D4rl: Datasets for deep data-driven reinforcement learning, 2020.
- Gu, J., Xiang, F., Li, X., Ling, Z., Liu, X., Mu, T., Tang, Y., Tao, S., Wei, X., Yao, Y., Yuan, X., Xie, P., Huang, Z., Chen, R., and Su, H. Maniskill2: A unified benchmark for generalizable manipulation skills. In *International Conference on Learning Representations*, 2023.
- Hafner, D., Lee, K.-H., Fischer, I., and Abbeel, P. Deep hierarchical planning from pixels. In Advances in Neural Information Processing Systems, 2022.
- Hakhamaneshi, K., Zhao, R., Zhan, A., Abbeel, P., and Laskin, M. Hierarchical few-shot imitation with skill transition models. In *International Conference on Learn*ing Representations, 2022.
- Hinton, G. Rmsprop optimizer. http://www.cs.
 toronto.edu/~tijmen/csc321/slides/
 lecture_slides_lec6.pdf.
- Hochreiter, S. and Schmidhuber, J. Long short-term memory. *Neural Computation*, 9(8):1735–1780, 1997.
- Huang, C., Guan, H., Jiang, A., Zhang, Y., Spratlin, M., and Wang, Y. Registration based few-shot anomaly detection. In *European Conference on Computer Vision (ECCV)*, 2022a.
- Huang, R., Yang, J., and Liang, Y. Safe exploration incurs nearly no additional sample complexity for reward-free RL. In *The Eleventh International Conference on Learning Representations*, 2023. URL https://openreview.net/forum?id=wNUgnln6esQ.
- Huang, X., Hu, Y., Luo, X., Han, J., Zhang, B., and Cao, X. Boosting variational inference with margin learning for few-shot scene-adaptive anomaly detection. *IEEE Transactions on Circuits and Systems for Video Technology*, pp. 1–1, 2022b.

- James, S., Bloesch, M., and Davison, A. J. Task-embedded control networks for few-shot imitation learning. In *Pro*ceedings of the Conference on Robot Learning, 2018.
- James, S., Freese, M., and Davison, A. J. Pyrep: Bringing v-rep to deep robot learning. arXiv preprint arXiv:1906.11176, 2019.
- James, S., Ma, Z., Arrojo, D. R., and Davison, A. J. Rlbench: The robot learning benchmark & learning environment. *IEEE Robotics and Automation Letters*, 5(2):3019–3026, 2020.
- Jiang, Y., Gupta, A., Zhang, Z., Wang, G., Dou, Y., Chen, Y., Fei-Fei, L., Anandkumar, A., Zhu, Y., and Fan, L. VIMA: Robot manipulation with multimodal prompts. In Proceedings of the 40th International Conference on Machine Learning, volume 202 of Proceedings of Machine Learning Research, pp. 14975–15022, 23–29 Jul 2023.
- Li, C., Zhang, R., Wong, J., Gokmen, C., Srivastava, S., Martín-Martín, R., Wang, C., Levine, G., Lingelbach, M., Sun, J., Anvari, M., Hwang, M., Sharma, M., Aydin, A., Bansal, D., Hunter, S., Kim, K.-Y., Lou, A., Matthews, C. R., Villa-Renteria, I., Tang, J. H., Tang, C., Xia, F., Savarese, S., Gweon, H., Liu, K., Wu, J., and Fei-Fei, L. BEHAVIOR-1k: A benchmark for embodied AI with 1,000 everyday activities and realistic simulation. In 6th Annual Conference on Robot Learning, 2022. URL https://openreview.net/forum?id=_8DoIe8G3t.
- Li, M., Canberk, A., Losey, D. P., and Sadigh, D. Learning human objectives from sequences of physical corrections. In 2021 IEEE International Conference on Robotics and Automation (ICRA), pp. 2877–2883, 2021. doi: 10.1109/ICRA48506.2021.9560829.
- Liu, H., Dass, S., Martín-Martín, R., and Zhu, Y. Modelbased runtime monitoring with interactive imitation learning, 2023a.
- Liu, J., He, L., Kang, Y., Zhuang, Z., Wang, D., and Xu, H. CEIL: Generalized contextual imitation learning. In *Thirty-seventh Conference on Neural Information Processing Systems*, 2023b. URL https://openreview.net/forum?id=suzMI2P1rT.
- Lu, C., Shi, J., and Jia, J. Abnormal event detection at 150 fps in matlab. In 2013 IEEE International Conference on Computer Vision, pp. 2720–2727, 2013.
- Lu, Y., Yu, F., Reddy, M. K. K., and Wang, Y. Few-shot scene-adaptive anomaly detection. In *European Conference on Computer Vision*, 2020.

- Mahadevan, V., Li, W., Bhalodia, V., and Vasconcelos, N. Anomaly detection in crowded scenes. In 2010 IEEE Computer Society Conference on Computer Vision and Pattern Recognition, pp. 1975–1981, 2010.
- Mandlekar, A., Xu, D., Wong, J., Nasiriany, S., Wang, C., Kulkarni, R., Fei-Fei, L., Savarese, S., Zhu, Y., and Martín-Martín, R. What matters in learning from offline human demonstrations for robot manipulation. In 5th Annual Conference on Robot Learning, 2021.
- Maron, O. and Lozano-Pérez, T. A framework for multiple-instance learning. In Jordan, M., Kearns, M., and Solla, S. (eds.), *Advances in Neural Information Processing Systems*, volume 10, 1997.
- Pang, G., Ding, C., Shen, C., and Hengel, A. v. d. Explainable deep few-shot anomaly detection with deviation networks. *arXiv preprint arXiv:2108.00462*, 2021.
- Park, D., Hoshi, Y., and Kemp, C. C. A multimodal anomaly detector for robot-assisted feeding using an lstm-based variational autoencoder. *IEEE Robotics and Automation Letters*, 3(3):1544–1551, 2018.
- Qiang, Y., Fei, S., and Jiao, Y. Anomaly detection based on latent feature training in surveillance scenarios. *IEEE Access*, 9:68108–68117, 2021.
- Robotics, C. Coppeliasim software. https://www.coppeliarobotics.com/.
- Roth, K., Pemula, L., Zepeda, J., Schölkopf, B., Brox, T., and Gehler, P. Towards total recall in industrial anomaly detection. In 2022 IEEE/CVF Conference on Computer Vision and Pattern Recognition (CVPR), pp. 14298–14308, 2022.
- Ruff, L., Vandermeulen, R., Goernitz, N., Deecke, L., Siddiqui, S. A., Binder, A., Müller, E., and Kloft, M. Deep one-class classification. In *Proceedings of the 35th International Conference on Machine Learning*, volume 80, pp. 4393–4402, 10–15 Jul 2018.
- Schroff, F., Kalenichenko, D., and Philbin, J. Facenet: A unified embedding for face recognition and clustering. In *The IEEE Conference on Computer Vision and Pattern Recognition (CVPR)*, June 2015.
- Sharma, P., Sundaralingam, B., Blukis, V., Paxton, C., Hermans, T., Torralba, A., Andreas, J., and Fox, D. Correcting Robot Plans with Natural Language Feedback. In *Proceedings of Robotics: Science and Systems*, New York City, NY, USA, June 2022. doi: 10.15607/RSS.2022. XVIII.065.
- Sheynin, S., Benaim, S., and Wolf, L. A hierarchical transformation-discriminating generative model for few

- shot anomaly detection. In 2021 IEEE/CVF International Conference on Computer Vision (ICCV), pp. 8475–8484, 2021.
- Shin, S., Lee, D., Yoo, M., Kim, W. K., and Woo, H. One-shot imitation in a non-stationary environment via multi-modal skill. In *Proceedings of the 40th International Conference on Machine Learning*, pp. 31562–31578, 23–29 Jul 2023.
- Song, Y., Wang, T., Cai, P., Mondal, S. K., and Sahoo, J. P. A comprehensive survey of few-shot learning: Evolution, applications, challenges, and opportunities. *ACM Comput. Surv.*, 55(13s), jul 2023. ISSN 0360-0300. doi: 10.1145/3582688. URL https://doi.org/10.1145/3582688.
- Sootla, A., Cowen-Rivers, A. I., Wang, J., and Ammar, H. B. Enhancing safe exploration using safety state augmentation. In Oh, A. H., Agarwal, A., Belgrave, D., and Cho, K. (eds.), *Advances in Neural Information Processing Systems*, 2022. URL https://openreview.net/forum?id=GH4q4WmGAs1.
- Sultani, W., Chen, C., and Shah, M. Real-world anomaly detection in surveillance videos. In 2018 IEEE/CVF Conference on Computer Vision and Pattern Recognition, pp. 6479–6488, 2018.
- Tao, S., Li, X., Mu, T., Huang, Z., Qin, Y., and Su, H. Abstract-to-executable trajectory translation for one-shot task generalization. In *Proceedings of the 40th International Conference on Machine Learning*, pp. 33850–33882, 2023.
- van der Maaten, L. and Hinton, G. Visualizing data using t-sne. *Journal of Machine Learning Research*, 9(86): 2579–2605, 2008.
- Wang, Z., Zhou, Y., Wang, R., Lin, T.-Y., Shah, A., and Lim, S.-N. Few-shot fast-adaptive anomaly detection. In Advances in Neural Information Processing Systems, 2022.
- Watahiki, H. and Tsuruoka, Y. One-shot imitation with skill chaining using a goal-conditioned policy in long-horizon control. In *ICLR 2022 Workshop on Generalizable Policy Learning in Physical World*, 2022.
- Wong, J., Tung, A., Kurenkov, A., Mandlekar, A., Fei-Fei, L., Savarese, S., and Martín-Martín, R. Error-aware imitation learning from teleoperation data for mobile manipulation. In 5th Annual Conference on Robot Learning, 2021.
- Yeh, J.-F., Chung, C.-M., Su, H.-T., Chen, Y.-T., and Hsu,W. H. Stage conscious attention network (scan): A demonstration-conditioned policy for few-shot imitation.

- In *Proceedings of the AAAI Conference on Artificial Intelligence*, volume 36, pp. 8866–8873, Jun. 2022.
- Yu, T., Finn, C., Dasari, S., Xie, A., Zhang, T., Abbeel, P., and Levine, S. One-shot imitation from observing humans via domain-adaptive meta-learning. In *Robotics: Science and Systems (RSS)*, 26-30 June 2018.
- Yu, T., Abbeel, P., Levine, S., and Finn, C. One-shot composition of vision-based skills from demonstration. In 2019 IEEE/RSJ International Conference on Intelligent Robots and Systems (IROS), pp. 2643–2650, 2019a.
- Yu, T., Quillen, D., He, Z., Julian, R., Hausman, K., Finn, C., and Levine, S. Meta-world: A benchmark and evaluation for multi-task and meta reinforcement learning. In *Conference on Robot Learning (CoRL)*, 2019b.
- Zhou, C. and Paffenroth, R. C. Anomaly detection with robust deep autoencoders. In *Proceedings of the 23rd ACM SIGKDD International Conference on Knowledge Discovery and Data Mining*, pp. 665–674, 2017.

Appendix

We present more details in this appendix, following a similar flow to the main paper. First, Section A introduces the few-shot imitation (FSI) policies. Then, more our PrObe's details are provided in Section B. Besides, we introduce the implemented AED baselines in Section C. Next, the designed multi-stage FSI tasks are exhaustively described in Section D, including task configurations, design motivations, and possible behavior errors. In addition, more experimental results are shown in Section E to support our claims. At last, we responsibly present the limitations of this work in Section F.

A. FSI Policy Details

We follow the main paper's Section 3 to implement three state-of-the-art demonstration-conditioned (DC) policies, including NaiveDC(James et al., 2018), DCT(Dance et al., 2021), and SCAN(Yeh et al., 2022), and monitor their behaviors.

Table 1. Gene	eral components' settings of FSI policies
	Visual head
input shape	$T\times4\times120\times160$
architecture	a resnet18 with a FC layer and a dropout layer
out dim. of resnet18	512
out dim. of visual head	256
dropout rate	0.5
	Actor
input dim.	512 or 768
architecture	a MLP with two parallel FC layers (pos & control)
hidden dims. of MLP	[512 or 768, 256, 64]
out dim. of pos layer	3
out dim. of control layer	1

Architecture settings The same visual head and actor architecture are employed for all policies to conduct a fair comparison. Table 1 and Table 2 present the settings of general components (visual head and actor) and respective task-embedding network settings for better reproducibility.

In the visual head, we added a fully-connected and a dropout layer after a single ResNet18 to avoid overfitting the data from base environments. Furthermore, the input dimension of the actor module depends on the sum of dimensions of the outputs from the visual head and the task-embedding network. For the DCT and SCAN policies, the task-embedding's dimension matches the visual head's output. However, the task-embedding's dimension in NaiveDC policy is twice the size.

Regarding the task-embedding network, NaiveDC concatenates the first and last frames of each demonstration and computes the average as the task-embedding, without involving any attention mechanism. In addition, DCT incorporates cross-demo attention to fuse demonstration features and then applies rollout-demo attention to compute the task-embedding. SCAN uses an attention mechanism to attend to each demonstration from the rollout, filtering out uninformative frames, and fuses them to obtain the final task-embedding. Furthermore, we use a standard LSTM, which differs from Yeh et al. (2022)'s setting.

Training details To optimize the policies, we utilize a RMSProp optimizer (Hinton) with a learning rate of 1e-4 and a L2 regularizer with a weight of 1e-2. Each training epoch involves iterating through all base environments. Within each iteration, we sample five demonstrations and ten rollouts from the sampled base environment. The total number of epochs varies depending on the specific tasks and is specified in Table 4. All policy experiments are conducted on a Ubuntu 20.04 machine equipped with an Intel i9-9900K CPU, 64GB RAM, and a NVIDIA RTX 3090 24GB GPU.

B. PrObe Details

In this work, we propose the Pattern Observer (PrObe) to address the novel AED task by detecting behavior errors from the policy's feature representations, which offers two advantages: (1) PrObe has a better understanding of the policy because the trained policy remains the same during both AED training and testing. This consistency enhances its effectiveness in identifying errors. (2) The additional task knowledge from the policy encoder aids in enhancing the error detection

Table 2. Task-embedding network settings of FSI policies

	NaiveDC
input data process out dim.	demonstrations concat the first and last demonstration frames and average 512
	DCT (Transformer-based)
input data process number of encoder layers number of decoder layers number of heads normalization eps dropout rate out dim.	current rollout and demonstrations a cross-demo attention followed by a rollout-demo attention 2 2 8 1e-5 0.1 256
	SCAN
input data process number of LSTM layer bi-directional LSTM out dim.	current rollout and demonstrations rollout-demo attentions for each demonstration and then average 1 False 256

performance. We have described PrObe's components and their usages in the main paper. Here, we introduce more details about the design of model architecture and training objectives.

Architecture design of PrObe The pattern extractor aims to extract the observable patterns from embeddings in policy features. To achieve this, we can leverage discrete encoding, as used in Hafner et al. (2022). However, the required dimension of discrete embedding might vary and be sensitive to the evaluation tasks. To address this, we leverage an alternative approach that operates in a continuous but sparse space. Besides, for the pattern flow generator, we use a standard LSTM model instead of a modern transformer. This is motivated by the characteristics of the AED task, where policy rollouts are collected sequentially, and adjacent frames contain crucial information when behavior errors occur. Thus, the LSTM model is better suited for addressing the AED task. The contributions of PrObe's components are verified and shown in Figure 12. From the results, our designed components significantly improve the performance.

Objectives We leverage three objectives to guide our PrObe: a BCE loss L_{cls} for error classification, a L1 loss L_{pat} for pattern enhancement, and a novel temporal-aware triplet loss L_{tem} for logit discernibility. First, the PrObe's error prediction \hat{y} can be optimized by L_{cls} since the ground-truth frame-level labels y are accessible during training, which is calculated by,

$$L_{cls} = -\frac{1}{N_r} \frac{1}{T_h} \sum_{i=0}^{N_r} \sum_{j=0}^{T_h} (y_{i,j} \cdot \ln \hat{y}_{i,j} + (1 - y_{i,j}) \cdot \ln(1 - \hat{y}_{i,j})), \tag{4}$$

where N_r and T_h are the number and length of rollouts, respectively. Then, we leverage the L1 objective L_{pat} to encourage the pattern extractor to learn a more sparse pattern embedding f_p , which can be formulated by

$$L_{pat} = \frac{1}{N_r} \frac{1}{T_h} \sum_{i=0}^{N_r} \sum_{j=0}^{T_h} |f_{p,i,j}|.$$
 (5)

With the objective L_{pat} , the pattern embeddings are expected to be sparse and easily observable of changes, benefiting the model in distinguishing behavior errors. Next, as previously pointed out, when applying contrastive learning to temporal-sequence data, the time relationship should also be considered, in addition to determining whether the frames are normal or errors for the task. Thus, L_{tem} is a novel temporal-aware triplet loss (Schroff et al., 2015), and the temporal-aware margin m_t in L_{tem} will have different effects depending on the relationship between the anchor and the positive/negative sample, as depicted in Figure 7. The L_{tem} can be calculated by:

Relationship between anchor and positive/negative sample

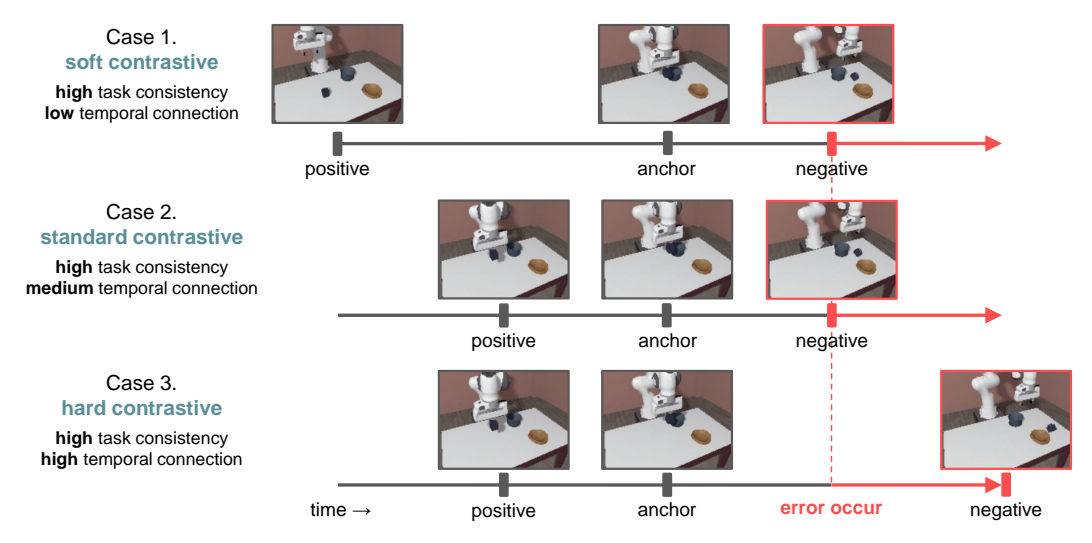


Figure 7. Schematic of our novel temporal-aware triplet loss L_{tem} . When the anchor and positive sample are more related in both the time and task aspects, the temporal-aware margin m_t will be larger (the closer the two embeddings are encouraged). Besides, m_t provides a slight encouragement in case the positive sample and anchor are far away on temporal distance.

$$L_{tem} = \frac{1}{N} \sum_{i=0}^{N} \max(\|\text{logit}_{i}^{a} - \text{logit}_{i}^{p}\|_{2} - \|\text{logit}_{i}^{a} - \text{logit}_{i}^{n}\|_{2} + m_{t}, 0),$$
(6)

where N is the number of sampled pairs, and the temporal-aware margin $m_t = m*(1.0 - \alpha*(d_{ap} - d_{an}))$ will be enlarged or reduced considering the temporal distance of anchor, positive and negative samples. Among them, m is the margin in the original triplet loss, and d_{ap} , d_{an} are the clipped temporal distances between the anchor and positive sample and the anchor and negative sample, respectively. With L_{tem} , PrObe can efficiently perform contrastive learning without getting confused by blindly pulling temporally distant anchors and positive samples closer. Lastly, the total loss L_{total} is the combination of three objectives:

$$L_{total} = \lambda_{pat} L_{pat} + \lambda_{tem} L_{tem} + \lambda_{cls} L_{cls}, \tag{7}$$

where λ_{pat} , λ_{tem} , and λ_{pat} are weights to balance different objectives.

C. Error Detector Details

We compare our PrObe with several strong baselines that possesses different attributes, aiming to verify their effectiveness on addressing the adaptable error detection (AED) task. In this section, we comprehensively present the attributes and training details associated with these baselines.

Table 3. Attributes of error detection methods policy training temporal DC-based method name output type dependent rollouts information **SVDDED** successful rollouts only distance to center **TaskEmbED** both probability **LSTMED** both probability **DCTED** both probability PrObe (ours) both probability

Baseline attributes Table 3 presents the attributes of AED baselines and our PrObe. All baselines have their own encoder and are independent of the policies, which offers the advantage that they only need to be trained once and can be used for various policies. However, as a result, they recognize errors only based on visual information. Now we describe their details:

- **SVDDED**: A modified one-class SVM method (Ruff et al., 2018) trained only with successful rollouts. It relies on measuring the distance between rollout embeddings to the center embedding to detect behavior errors, without considering the temporal information. We average demonstration features as the center embedding and minimize the embedding distance between rollout features and the center during training.
- TaskEmbED: A single-frame baseline trained with successful and failed rollouts, which is a modification from the NaiveDC policy (James et al., 2018). It concatenates and averages the first and last demonstration frames as the task-embedding. Then, it predicts the behavior errors conditioned on the current frame and task-embedding.
- LSTMED: A standard LSTM model (Hochreiter & Schmidhuber, 1997) predicts errors based solely on the current rollout. It is trained with successful and failed rollouts with no demonstration knowledge provided. It is expected to excel in identifying errors that occur at similar timings to those observed during training. However, it may struggle to recognize errors that deviate from the demonstrations.
- **DCTED**: A baseline with temporal information derived from the DCT policy (Dance et al., 2021). It is trained with successful and failed rollouts and incorporates with demonstration information. One notable distinction between DCTED and our PrObe lies in their policy dependencies. DCTED detects errors using its own encoder, which solely leverages visual information obtained within the novel environment. Conversely, PrObe learns within the policy feature space, incorporating additional task-related knowledge.

Training details Similar to optimizing the policies, we utilize a RMSProp optimizer with a learning rate of 1e-4 and a weight regularizer with a weight of 1e-2 to train the error detection models. During each iteration within an epoch, we sample five demonstrations, ten successful agent rollouts, and ten failed rollouts from the sampled base environment for all error detection models except SVDDED. For SVDDED, we sample five demonstrations and twenty successful agent rollouts since it is trained solely on normal samples. Notably, all error detection experiments are conducted on the same machine as the policy experiments, ensuring consistency between the two sets of experiments.

D. Evaluation Tasks

To obtain accurate frame-level error labels in the base environments and to create a simulation environment that closely resembles real-world scenarios, we determined that existing robot manipulation benchmarks/tasks (Yu et al., 2019b; James et al., 2020; Fu et al., 2020; Mandlekar et al., 2021; Yeh et al., 2022; Li et al., 2022; Gu et al., 2023) did not meet our requirements. Consequently, seven challenging FSI tasks containing 329 base and 158 novel environments are developed. Their general attributes are introduced in Section D.1 and Table 4; the detailed task descriptions and visualizations are provided in Section D.2 and Figure 8-9, respectively.

D.1. General Task Attributes

- Generalization: To present the characteristics of changeable visual signals in real scenes, we build dozens of novel environments for each task, comprising various targets and task-related or environmental distractors. Also, Dozens of base environments are built as training resources, enhancing AED methods' generalization ability. Letting them train in base environments with different domains can also be regarded as a domain randomization technique (Bonardi et al., 2020), preprocessing for future sim2real experiments.
- Challenging: Three challenges, including multi-stage tasks, misaligned demonstrations, and different appearances between expert and agent, are included in our FSI tasks. Moreover, unlike existing benchmarks (e.g., RLBench (James et al., 2020)) attaching the objects to the robot while grasping, we turn on the gravity and friction during the whole process of simulation, so grasped objects may drop due to unsmooth movement.
- **Realistic**: Our tasks support multi-source lighting, soft shadow, and complex object texture to make them closer to reality (see Figure 9). Existing benchmarks usually have no shadow (or only a hard shadow) and simple texture. The gravity and friction stated above also make our tasks more realistic.

Table 4. FSI task configuration	ions
---------------------------------	------

Task	# of stages	# of epochs	# of base env.	# of novel env.	# of task distractors	# of env. distractors
Close Drawer	1	160	18	18	1	3
Press Button	1	40	27	18	0	3
Pick & Place	2	50	90	42	1	0
Move Glass Cup	2	50	49	25	1	0
Organize Table	3	50	49	25	1	0
Back to Box	3	50	60	18	0	3
Factory Packing	4	80	36	12	0	0

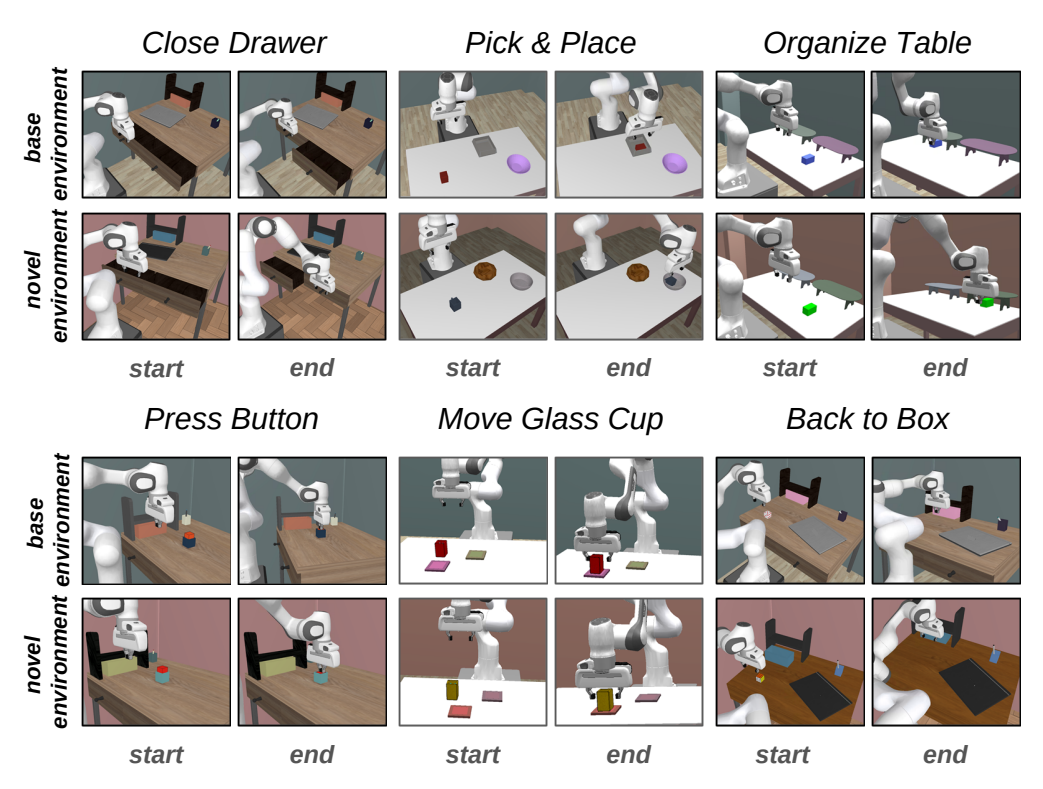


Figure 8. Visualizations of our designed indoor FSI tasks. The backgrounds (wall, floor) and interactive objects are disjoint between base and novel environments.

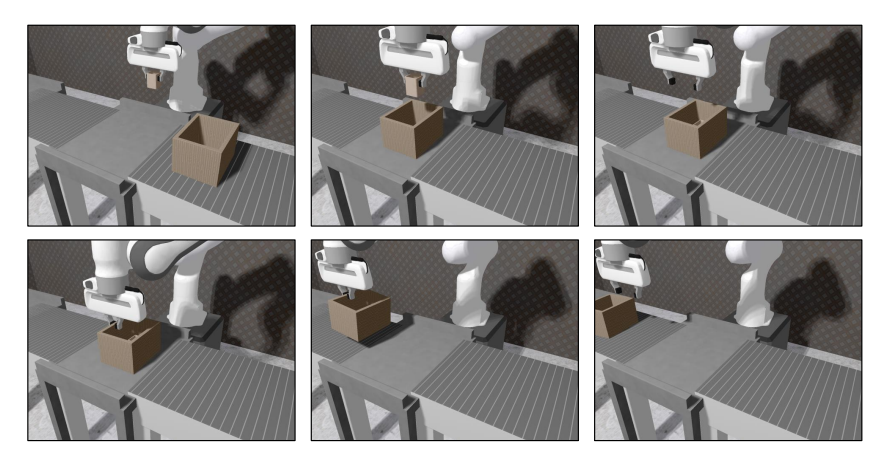


Figure 9. Progress visualization of our Factory Packing task. The agent needs to wait for the box's arrival. It then places the product into the box and lets the box move to the next conveyor belt.

D.2. Task Descriptions

	Close Drawer (1-stage, indoor)
Description	Fully close the drawer that was closed by the expert in demonstrations. Besides, the
•	objects on the table will be randomly set in the designated area.
Success condition	The target drawer is fully closed, and another drawer (distractor) must not be moved.
Behavior errors	(1) Not fully close the target drawer; (2) Close the distractor, not the target drawer; (3) Close two drawers at the same time.
	Press Button (1-stage, indoor)
Description	Fully press the button which is randomly placed in a designated area.
Success condition	The button is fully pressed.
Behavior errors	(1) Not touching the button at all; (2) The button is not fully pressed.
	Pick & Place (2-stages, indoor)
Description	Pick and place the mug/cup into the bowl the expert placed in demonstrations.
Success condition	The mug/cup is fully placed in the target bowl.
Behavior errors	(1) Failed to pick up the mug/cup; (2) Failed to place it into the target bowl; (3) Misplaced the mug/cup into another bowl (distractor).
	Move Glass Cup (2-stages, indoor)
Description	Pick up and place a glass of water on the coaster the expert placed in demonstrations.
Success condition	The glass of water is placed on the target coaster and no water is spilled.
Behavior errors	(1) Failed to pick up the glass of water; (2) drips spilling; (3) Not placed on the target coaster.
	Organize Table (3-stages, indoor)
Description	Pick up and place the object in front of the target bookshelf, and push it under the shelf.
Success condition	The object is fully under the target shelf.
Behavior errors	(1) Failed to pick up the object; (2) Losing object during moving; (3) Not fully placed under the target shelf.
	Back to Box (3-stages, indoor)
Description	Pick up the magic cube/dice and place it into the storage box. Then, push the box until it is fully under the bookshelf.
Success condition	The magic cube/dice is in the storage box, and the box is fully under the bookshelf.
Behavior errors	(1) Failed to pick up the magic cube/dice. (2) Failed to place the magic cube/dice into the storage box. (3) The box is not fully under the bookshelf.
	Factory Packing (4-stages, factory)
Description	Wait until the product box reaches the operating table, place the product in the box, and pick and place the box on the next conveyor belt.
Success condition	The product is inside the box, and the box reaches the destination table.
Behavior errors	(1) Failed to place the product into the box. (2) Failed to pick up the box. (3) Failed to place the box on the next conveyor belt.

E. Additional Experimental Results

This section reports more experimental results. We introduce the accuracy function used for determining an error prediction result in Section E.1. Furthermore, more details on the main experiment are provided in Section E.2, Next, all ablations are summarized in Section E.3. At last, the pilot study on error correction is shown in Section E.4.

E.1. Accuracy Function in Our AED task

rollout successful?	any error raised?	marked as
√	✓	false positive (FP)
\checkmark	×	true negative (TN)
×	\checkmark	true positive (TP)
×	×	false negative (FN)

Figure 10. Rules of the accuracy function $A(\cdot,\cdot)$ to determine the error prediction results.

As stated in the main paper, the frame-level label is lacking during inference because novel environments only indicate whether the current rollout is a success or failure. Hence, we follow similar rules in Wong et al. (2021) to define the accuracy function $A(\cdot, \cdot)$, i.e., how to determine the error prediction outcome, as elaborated in Figure 10. The $A(\cdot, \cdot)$ determines the prediction result at the sequence-level, which may not sufficiently reflect whether the timing to raise the error is accurate. Thus, we further conduct the timing accuracy experiment (Figure 5 in the main paper).

E.2. Main Experiment's Details

Table 5. FSI policy performance. Success rate (SR) [\uparrow] and its standard deviation (STD) are reported. Notably, STD is calculated across novel environments, rather than multiple experiment rounds. That's also the reason that some STD values are large, as the difficulty of different novel environments in the same task varies.

	Close Drawer	Press Button	Pick & Place	Organize Table
NaiveDC DCT	$91.11 \pm 20.85\%$ $80.56 \pm 26.71\%$	$51.94 \pm 18.79\%$ $80.56 \pm 11.65\%$	$55.00 \pm 24.98\%$ $64.05 \pm 19.77\%$	$12.20 \pm 13.93\%$ 79.00 ± 09.27 %
SCAN	$88.33 \pm 13.94\%$	$75.56 \pm 12.68\%$	$71.19 \pm 15.38\%$	$66.60 \pm 23.18\%$
	Move Glass Cup	Back to Box	Factory Packing	
NaiveDC DCT SCAN	$39.00 \pm 28.63\%$ $51.80 \pm 23.99\%$ $72.60 \pm 11.84\%$	$08.89 \pm 09.21\%$ $29.17 \pm 09.46\%$ $\mathbf{58.89 \pm 10.87}\%$	$45.42 \pm 30.92\%$ $88.75 \pm 07.11\%$ $63.75 \pm 33.11\%$	

FSI policy performance The policy performance is originally reported in Figure 4 of the main paper. Here, we provide a comprehensive overview in Table 5. The policy conducts 20 executions (rollouts) for each novel environment to obtain the success rate (SR). Then, the average success rate and its standard deviation (STD) are calculated across those SRs. Some large STD values are due to the variety in difficulty among novel environments. Factors such as variations in object size or challenging destination locations can lead to different performance outcomes for the policies. Additionally, these collected rollouts are also used for later AED inference.

In general, the NaiveDC policy achieves the best results in the simplest tasks because the task-embedding from the concatenation of the first and last two frames provides sufficient information. However, its performance rapidly declines as task difficulty increases. On the other hand, the DCT policy excels in tasks where the misalignment between demonstrations is less severe, as it fuses the task-embeddings in the temporal dimension. Lastly, the SCAN policy outperforms in more difficult tasks because its attention mechanism filters out uninformative demonstration frames.

Main experiment's detailed values and ROC curves The main experiment result is originally reported in Figure 4 of the main paper. Here, Table 8 and Figure 15 present its detailed values and ROC curves, which better demonstrate our PrObe's performance gap against other methods. To highlight again, our proposed PrObe obtains the best performance on both metrics and can handle the various behaviors from different policies.

E.3. Ablation Study

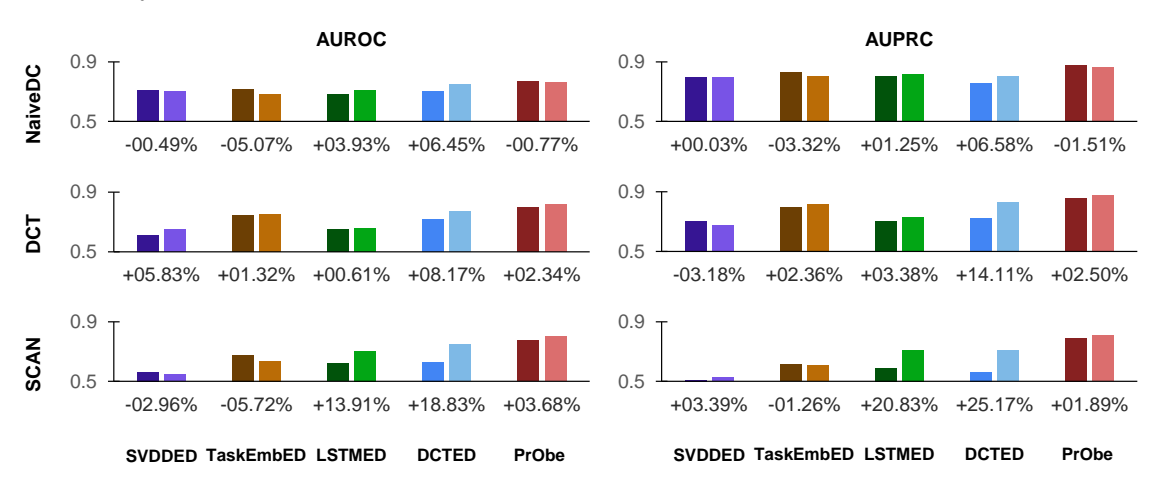


Figure 11. Effectiveness of rollout augmentation (RA). $AUROC[\uparrow]$ and $AUPRC[\uparrow]$ are reported. Methods trained without RA (dark) and with RA(bright) and their performance gap are listed. RA is more beneficial for methods with time information (rightmost three columns). Also, the improvement from RA is more evident when the performance of FSI policy is higher (SCAN case).

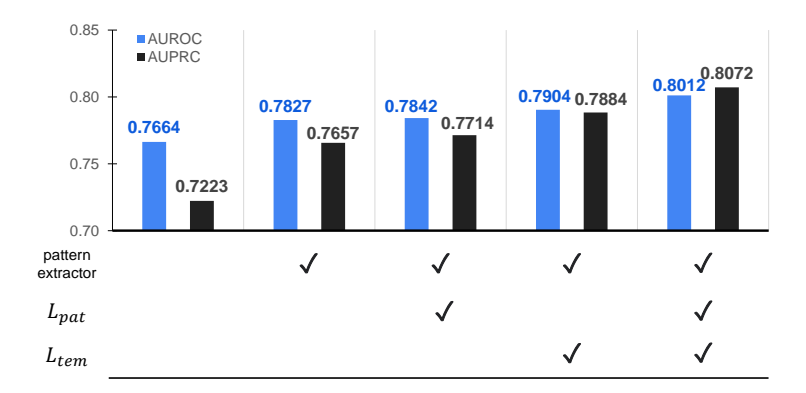


Figure 12. Component contributions. $AUROC[\uparrow]$ and $AUPRC[\uparrow]$ are reported. The pattern extractor and two auxiliary objectives significantly improve the performance.

Rollout augmentation As stated before, the collected agent rollouts exhibit limited diversity. This experiment aims to validate whether rollout augmentation (RA) enhances the rollout diversity and, consequently, improves the robustness of error detectors. In Figure 11, we present the results of all error detection methods (trained with and without RA) monitoring policies solving the *Pick & Place* task, yielding the following findings: (1) RA has a minor or even negative impact on SVDDED, as expected. Since SVDDED is exclusively trained on (single) frames from successful rollouts, the removal of frames by RA decreases overall frame diversity. (2) RA proves beneficial for methods incorporating temporal information (LSTMED, DCTED, and PrObe), particularly when the FSI policy performs better (SCAN case). This is because error detectors cannot casually trigger an error, or they risk making a false-positive prediction. The results indicate that methods trained with RA generate fewer false-positive predictions, showcasing improved robustness to various policy behaviors.

Contribution of PrObe components Figure 12 illustrates the performance contribution of each PrObe's component, resulting from monitoring the SCAN policy solving the *Pick & Plcae* task. The naive model (first column) removes the pattern extractor and uses a FC layer followed by an IN layer to transform history embeddings. Obviously, the designed components and objectives boost performance, especially when adding the pattern extractor into the model. We attribute this to the fact that extracted embedding (representation) patterns by our components are more informative and discernible.

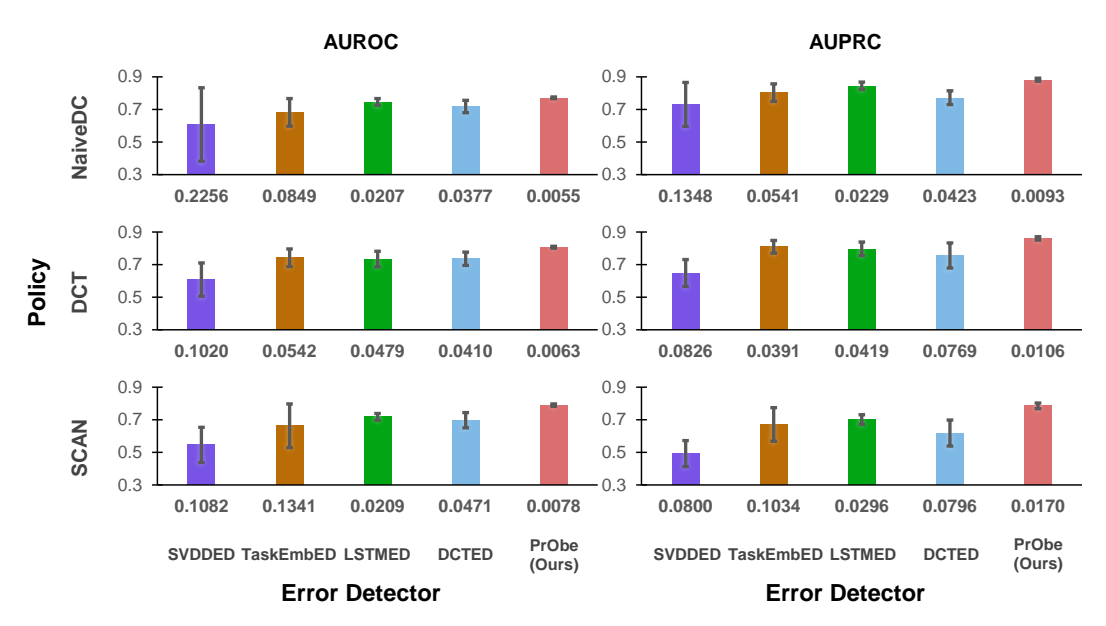


Figure 13. Performance results with error bars (standard deviation, STD). $\mathbf{AUROC}[\uparrow]$, $\mathbf{AUPRC}[\uparrow]$ are reported. Here, STDs are computed across multiple experiment rounds (random seeds). It is obvious that in the representative *Pick* & *Place* task, PrObe not only achieves the highest scores when detecting all policies' behavior errors but also has the best stability (the smallest STD).

Table 6. Demonstration quality experiment. **AUROC** [↑] is reported. This experiment verifies the influence of demonstration quality on both the FSI policy and AED methods. PrObe is the only method that can achieve higher performance when receiving sub-optimal demonstrations, as the FSI policies raise more failures.

	1	NaiveDC polic	су			
Setting	Success Rate	SVDDED	TaskEmbED	LSTMED	DCTED	PrObe
All optimal	$51.94 \pm 18.79\%$	0.6956	0.7280	0.7051	0.8405	0.8851
3 optimal & 2 sub-optimal	$50.83 \pm 18.50\%$	0.6861	0.7407	0.7168	0.8832	0.9059
All sub-optimal	$51.67 \pm 17.24\%$	0.6414	0.7276	0.7044	0.8446	0.8930
		DCT policy				
Setting	Success Rate	SVDDED	TaskEmbED	LSTMED	DCTED	PrObe
All optimal	$80.56 \pm 11.65\%$	0.3789	0.3597	0.4468	0.5734	0.7474
3 optimal & 2 sub-optimal	$78.61 \pm 14.02\%$	0.3908	0.3811	0.4606	0.6019	0.7530
All sub-optimal	$77.22 \pm 14.16\%$	0.3899	0.4051	0.4718	0.5341	0.7588
		SCAN policy	7			
Setting	Success Rate	SVDDED	TaskEmbED	LSTMED	DCTED	PrObe
All optimal	$75.56 \pm 12.68\%$	0.4653	0.4657	0.4487	0.6757	0.7505
3 optimal & 2 sub-optimal	$71.67 \pm 11.18\%$	0.4985	0.5165	0.4979	0.7467	0.7804
All sub-optimal	$69.72 \pm 12.30\%$	0.4886	0.5262	0.5096	0.7140	0.7752

Performance stability Our work involves the training and testing of all policies and AED methods to produce results for an FSI task. Additionally, each task comprises numerous base and novel environments. These factors make it time-consuming and impractical to include error bars in the main experiment (Figure 4 of the main paper). Based on our experience, generating the results of the main experiment once would require over 150 hours.

Therefore, we selected the most representative *Pick & Place* task among our FSI tasks and conducted multiple training and inference iterations for all AED methods. We present the AUROC, AUPRC, and their standard deviations averaged over multiple experimental rounds (with five random seeds) in Figure 13. From the results, our proposed PrObe not only achieves the best performance in detecting behavior errors across all policies but also exhibits the most stable performance among all AED methods, with the smallest standard deviation (STD) values.

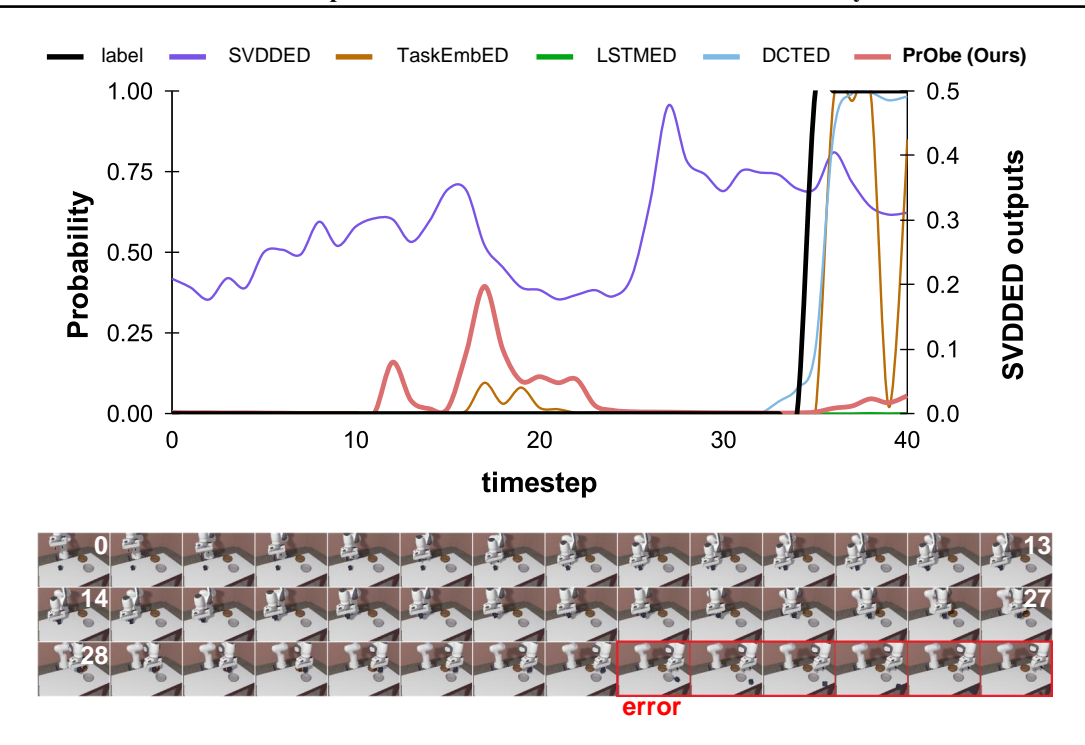


Figure 14. PrObe's failure prediction. In the *Pick & Place* task, the rollout is terminated immediately if the mug is no longer on the table, which means the error detectors have only six frames to detect the error in this case. However, it took a while for our Probe's pattern flow to cause enough change. By the last frame, ProObe was just about to increase its predicted probability, but it was too late.

Demonstration quality In this experiment, we aim to verify the influence of demonstration quality on both the FSI policy and AED methods. We test it on the *Press Button* task. We collect sub-optimal demonstrations that failed to press the button at the first trial but pressed the button successfully on the second try. We provide these sub-optimal demonstrations and let the policies and AED methods perform the task.

Specifically, the policy performance should drops when the demonstration quality decreases. As a result, the AED methods should get a higher AUPRC score if they are not affected by the quality changes of demonstrations since it's easier to find an error. However, from Table 6, we can observe that not all AED methods obtain higher scores, meaning that they are also affected by the quality decreasing. Notably, our proposed PrObe is the only method that achieves better results for all cases - compare the first and second rows and the first and third rows for each policy. Additionally, an interesting observation can be found in the case of NaiveDC policy (all optimal vs. all sub-optimal): The LSTMED and the TaskEmbED obtained similar AUPRC scores, as they don't access the demonstration information; SVDDED baseline suffered in this situation since it averages every demonstration frame (including those from sub-optimal demonstrations); DCTED and our PrObe get a slightly better result because they filter useful information from demonstrations.

Case study on PrObe's failure prediction We analyze the cases in which PrObe is poor at detecting behavior errors and visualize the results in Figure 14. As stated in the main paper, our PrObe requires a short period after the error occurs to allow the pattern flow to cause enough changes. However, in the Figure 14 case, the mug had fallen off the table, causing this rollout to be stopped immediately. Such a short time is insufficient for PrObe to reflect adequately, rendering it unable to (substantially) increase the prediction probability of behavioral errors at the last moment. Developing mechanisms for quick responsive pattern flow is one of our future research directions.

E.4. Pilot Study on Eeror Correction

To further examine the practicality of our AED task, we conducted a pilot study on error correction. In this experiment, the FSI policy is paused after the AED methods detect an error. Then, a correction policy from Wong et al. (2021), which resets the agent to a predefined safe pose, is applied. At last, the FSI policy continues to complete the task.

Table 7. Error correction results. **Success Rate** (**SR**) [\uparrow] is reported. The detection threshold is set as 0.9 for all compared methods. The values indicate the performance of the DCT policy without correction (first column) and its collaboration with the correction policy and four AED methods (remaining columns). PrObe is the only method that improves the performance, as it detects the error most accurately.

DCT policy	w/ TaskEmbED	w/ LSTMED	w/ DCTED	w/ PrObe
$80.56 \pm 11.65\%$	$80.56 \pm 11.65\%$	$80.28 \pm 11.60\%$	$71.67 \pm 20.75\%$	$\bf 82.22 \pm 10.17\%$

We conducted the study on the *Press Button* task, which will most likely be corrected after an error occurs. In this task, the correction policy is defined as moving to the top center of the table. We let the DCT policy cooperate with the correction policy and four AED methods (SVDDED excluded), as summarized in Table 7. We have two findings from the results: (1) Our PrObe is verified to be the most accurate method again. In contrast, other AED methods will cause errors at the wrong timing, so the correction policy cannot improve performance (it may even have a negative impact on original successful trials). (2) The performance gain from the correction policy is minor since it lacks precise guidance in unseen environments.

We believe error correction in novel environments deserves a separate study due to its challenging nature, as observed in the pilot study. One potential solution is the human-in-the-loop correction, which operates through instructions (Sharma et al., 2022; Cui et al., 2023) or physical guidance (Li et al., 2021). However, their generalization ability and cost when applying to our AED task need further discussion and verification. We will leave this as a topic for our future work.

F. Limitations

Offline evaluation for the main experiment? Our ultimate goal is to terminate (or pause) the policy instantly when detecting a behavior error online. However, in our main experiment, only the trained policies performed in novel environments online, and their rollouts were collected. AED methods later use the rollouts to predict errors for a fair comparison. Nevertheless, we illustrate that PrObe effectively address the online detection challenge through the time accuracy experiment. Additionally, the pilot study on error correction involves running AED methods online to promptly correct errors.

No state-of-the-art (SOTA) baselines for the AED task? As we formulate the novel AED task, there is no existing method that fits the task. We have found that some SOTA works (Li et al., 2021; Sharma et al., 2022; Cui et al., 2023; Liu et al., 2023a) also address the error detection or correction task in robotics. However, ours and theirs have different natures in terms of the task scenario. They usually require human-in-the-loop guidance, while in our setting, the robot is in an unseen environment, and the expert may only have the ability to perform demonstrations but is unable to correct the robot's failures.

Additionally, we have made efforts to design baselines with different characteristics, as listed in Table 3. Our baselines include a traditional recurrent network, a one-class SVM, a metric-learning method, and a powerful transformer model. Notably, PrObe demonstrates superior performance compared to the baselines in our extensive experiments.

Not evaluated on benchmarks or in real-world environments? Due to the practical challenges inherent in FSI tasks and the AED task, none of the existing robot manipulation benchmarks align with our specific requirements. For instance, FSI tasks necessitate multi-stage scenarios or variations in configurations and appearances between experts and agents. In the case of AED, it is crucial to gather failed rollouts in the base environments efficiently. As a result, we have had to develop our own environments and tasks. Moreover, the lack of real-world experiments is attributed to the following reasons: (1) Deploying the necessary resources for the AED task in the real world is high-cost and requires a long-term plan due to safety concerns. (2) The FSI policies still struggle to perform complex tasks in the real world, making assessments less than comprehensive. (3) Although PrObe achieves the best performance, there is still significant room for improvement in addressing the AED task.

We emphasize that rashly conducting AED and FSI research in real environments may cause irreparable damage. Even previous error correction work (Wong et al., 2021) or related safe exploration research (Sootla et al., 2022; Anderson et al., 2023; Huang et al., 2023) was conducted in simulation environments, demonstrating that it is reasonable and valuable for us to conduct detailed verification in simulations first. As mentioned earlier, we have developed seven challenging and realistic multi-stage FSI tasks, each containing dozens of base and novel environments. To our knowledge, the simulation environments we established are the closest to the real scenarios in the literature.

Table 8. AED methods' performance on our seven challenging FSI tasks. The value under the policy indicates the policy's success rate in that task. Our proposed PrObe demonstrates its superiority among all the methods on both metrics and is the most robust method for different policies.

		С	lose Draw	or	I	Press Butto	n
Metric [↑]	AED	NaiveDC	DCT	SCAN	NaiveDC	DCT	SCAN
		91.11%	80.56%	88.33%	51.94%	80.56%	75.56%
	SVDDED	0.7404	0.8378	0.4079	0.4113	0.5710	0.4280
	TaskEmbED	0.8395	0.7081	0.6498	0.4872	0.5429	0.4754
AUROC	LSTMED	0.8186	0.6590	0.7867	0.3769	0.4886	0.4066
	DCTED	0.8250	0.6413	0.7218	0.7194	0.7306	0.7491
	PrObe	0.9133	0.7680	0.6978	0.7957	0.7506	0.7782
	SVDDED	0.2626	0.7039	0.1411	0.6956	0.3789	0.4653
	TaskEmbED	0.6840	0.5995	0.2220	0.7280	0.3597	0.4657
AUPRC	LSTMED	0.7700	0.6493	0.6677	0.7051	0.4468	0.4487
	DCTED	0.7813	0.6739	0.6390	0.8405	0.5734	0.6757
	PrObe	0.8350	0.7438	0.5829	0.8851	0.7474	0.7505
		P	ick & Plac	ce	Мо	ve Glass (Сир
Metric [↑]	AED	NaiveDC	DCT	SCAN	NaiveDC	DCT	SCAN
		55.00%	64.05%	71.19%	39.00%	51.80%	72.60%
	SVDDED	0.7074	0.6125	0.5646	0.4447	0.6201	0.6473
	TaskEmbED	0.6810	0.7523	0.6381	0.8370	0.5779	0.7950
AUROC	LSTMED	0.7116	0.6555	0.7050	0.8086	0.6670	0.6804
	DCTED	0.7493	0.7743	0.7482	0.7143	0.5954	0.6401
	PrObe	0.7635	0.8173	0.8012	0.7487	0.6697	0.7425
	SVDDED	0.7971	0.7001	0.5078	0.8323	0.7188	0.6251
ALIDDG	TaskEmbED	0.8028	0.8173	0.6065	0.9609	0.6823	0.8204
AUPRC	LSTMED	0.8148	0.7304	0.7103	0.9420	0.7720	0.6404
	DCTED PrObe	0.8041 0.8665	0.8294 0.8780	0.7063 0.8072	0.9012 0.9228	0.7086 0.7907	0.5713 0.7495
	riobe	0.0005	0.0700	0.0072	0.9228	0.7907	0.7493
3.6	A.E.D.		ganize Tal			Back to Bo.	
Metric [†]	AED	NaiveDC	DCT	SCAN	NaiveDC	DCT	SCAN
Metric [†]		NaiveDC 12.20%	DCT 79.00%	SCAN 66.60%	NaiveDC 08.89%	DCT 29.17%	SCAN 58.89%
Metric [†]	SVDDED	NaiveDC 12.20% 0.2581	DCT 79.00% 0.5622	SCAN 66.60% 0.5000	NaiveDC 08.89% 0.4621	DCT 29.17% 0.5537	SCAN 58.89% 0.5498
	SVDDED TaskEmbED	NaiveDC 12.20% 0.2581 0.8078	DCT 79.00% 0.5622 0.6382	SCAN 66.60% 0.5000 0.6193	NaiveDC 08.89% 0.4621 0.3221	DCT 29.17% 0.5537 0.7220	SCAN 58.89% 0.5498 0.7041
Metric [†]	SVDDED TaskEmbED LSTMED	NaiveDC 12.20% 0.2581 0.8078 0.5946	DCT 79.00% 0.5622 0.6382 0.7001	SCAN 66.60% 0.5000 0.6193 0.6734	NaiveDC 08.89% 0.4621 0.3221 0.4148	DCT 29.17% 0.5537 0.7220 0.7707	SCAN 58.89% 0.5498 0.7041 0.8237
	SVDDED TaskEmbED LSTMED DCTED	NaiveDC 12.20% 0.2581 0.8078 0.5946 0.5844	DCT 79.00% 0.5622 0.6382 0.7001 0.6702	SCAN 66.60% 0.5000 0.6193 0.6734 0.5962	NaiveDC 08.89% 0.4621 0.3221 0.4148 0.6022	DCT 29.17% 0.5537 0.7220 0.7707 0.4772	SCAN 58.89% 0.5498 0.7041 0.8237 0.7489
	SVDDED TaskEmbED LSTMED DCTED PrObe	NaiveDC 12.20% 0.2581 0.8078 0.5946 0.5844 0.6808	DCT 79.00% 0.5622 0.6382 0.7001 0.6702 0.6550	SCAN 66.60% 0.5000 0.6193 0.6734 0.5962 0.6759	NaiveDC 08.89% 0.4621 0.3221 0.4148 0.6022 0.8446	DCT 29.17% 0.5537 0.7220 0.7707 0.4772 0.7276	SCAN 58.89% 0.5498 0.7041 0.8237 0.7489 0.8614
	SVDDED TaskEmbED LSTMED DCTED PrObe SVDDED	NaiveDC 12.20% 0.2581 0.8078 0.5946 0.5844 0.6808 0.8911	DCT 79.00% 0.5622 0.6382 0.7001 0.6702 0.6550 0.4800	SCAN 66.60% 0.5000 0.6193 0.6734 0.5962 0.6759	NaiveDC 08.89% 0.4621 0.3221 0.4148 0.6022 0.8446	DCT 29.17% 0.5537 0.7220 0.7707 0.4772 0.7276 0.8652	SCAN 58.89% 0.5498 0.7041 0.8237 0.7489 0.8614 0.6433
AUROC	SVDDED TaskEmbED LSTMED DCTED PrObe SVDDED TaskEmbED	NaiveDC 12.20% 0.2581 0.8078 0.5946 0.5844 0.6808 0.8911 0.9786	DCT 79.00% 0.5622 0.6382 0.7001 0.6702 0.6550 0.4800 0.3922	SCAN 66.60% 0.5000 0.6193 0.6734 0.5962 0.6759 0.5086 0.4865	NaiveDC 08.89% 0.4621 0.3221 0.4148 0.6022 0.8446 0.9367 0.9375	DCT 29.17% 0.5537 0.7220 0.7707 0.4772 0.7276 0.8652 0.9314	SCAN 58.89% 0.5498 0.7041 0.8237 0.7489 0.8614 0.6433 0.7401
	SVDDED TaskEmbED LSTMED DCTED PrObe SVDDED	NaiveDC 12.20% 0.2581 0.8078 0.5946 0.5844 0.6808 0.8911	DCT 79.00% 0.5622 0.6382 0.7001 0.6702 0.6550 0.4800	SCAN 66.60% 0.5000 0.6193 0.6734 0.5962 0.6759	NaiveDC 08.89% 0.4621 0.3221 0.4148 0.6022 0.8446	DCT 29.17% 0.5537 0.7220 0.7707 0.4772 0.7276 0.8652	SCAN 58.89% 0.5498 0.7041 0.8237 0.7489 0.8614 0.6433
AUROC	SVDDED TaskEmbED LSTMED DCTED PrObe SVDDED TaskEmbED LSTMED	NaiveDC 12.20% 0.2581 0.8078 0.5946 0.5844 0.6808 0.8911 0.9786 0.9611	DCT 79.00% 0.5622 0.6382 0.7001 0.6702 0.6550 0.4800 0.3922 0.6352	SCAN 66.60% 0.5000 0.6193 0.6734 0.5962 0.6759 0.5086 0.4865 0.6356	NaiveDC 08.89% 0.4621 0.3221 0.4148 0.6022 0.8446 0.9367 0.9375 0.9555	DCT 29.17% 0.5537 0.7220 0.7707 0.4772 0.7276 0.8652 0.9314 0.9546	SCAN 58.89% 0.5498 0.7041 0.8237 0.7489 0.8614 0.6433 0.7401 0.8913
AUROC	SVDDED TaskEmbED LSTMED DCTED PrObe SVDDED TaskEmbED LSTMED DCTED	NaiveDC 12.20% 0.2581 0.8078 0.5946 0.5844 0.6808 0.8911 0.9786 0.9611 0.9452 0.9652	DCT 79.00% 0.5622 0.6382 0.7001 0.6702 0.6550 0.4800 0.3922 0.6352 0.5905	SCAN 66.60% 0.5000 0.6193 0.6734 0.5962 0.6759 0.5086 0.4865 0.6356 0.5255 0.6983	NaiveDC 08.89% 0.4621 0.3221 0.4148 0.6022 0.8446 0.9367 0.9375 0.9555 0.9679	DCT 29.17% 0.5537 0.7220 0.7707 0.4772 0.7276 0.8652 0.9314 0.9546 0.8534 0.9438	SCAN 58.89% 0.5498 0.7041 0.8237 0.7489 0.8614 0.6433 0.7401 0.8913 0.7880
AUROC	SVDDED TaskEmbED LSTMED DCTED PrObe SVDDED TaskEmbED LSTMED DCTED PrObe	NaiveDC 12.20% 0.2581 0.8078 0.5946 0.5844 0.6808 0.8911 0.9786 0.9611 0.9452 0.9652	DCT 79.00% 0.5622 0.6382 0.7001 0.6702 0.6550 0.4800 0.3922 0.6352 0.5515 0.5905	SCAN 66.60% 0.5000 0.6193 0.6734 0.5962 0.6759 0.5086 0.4865 0.6356 0.5255 0.6983	NaiveDC 08.89% 0.4621 0.3221 0.4148 0.6022 0.8446 0.9367 0.9375 0.9555 0.9679 0.9903	DCT 29.17% 0.5537 0.7220 0.7707 0.4772 0.7276 0.8652 0.9314 0.9546 0.8534 0.9438 Statistics	SCAN 58.89% 0.5498 0.7041 0.8237 0.7489 0.8614 0.6433 0.7401 0.8913 0.7880 0.9097
AUROC	SVDDED TaskEmbED LSTMED DCTED PrObe SVDDED TaskEmbED LSTMED DCTED	NaiveDC 12.20% 0.2581 0.8078 0.5946 0.5844 0.6808 0.8911 0.9786 0.9611 0.9452 0.9652	DCT 79.00% 0.5622 0.6382 0.7001 0.6702 0.6550 0.4800 0.3922 0.6352 0.5905	SCAN 66.60% 0.5000 0.6193 0.6734 0.5962 0.6759 0.5086 0.4865 0.6356 0.5255 0.6983	NaiveDC 08.89% 0.4621 0.3221 0.4148 0.6022 0.8446 0.9367 0.9375 0.9555 0.9679	DCT 29.17% 0.5537 0.7220 0.7707 0.4772 0.7276 0.8652 0.9314 0.9546 0.8534 0.9438 Statistics	SCAN 58.89% 0.5498 0.7041 0.8237 0.7489 0.8614 0.6433 0.7401 0.8913 0.7880
AUROC	SVDDED TaskEmbED LSTMED DCTED PrObe SVDDED TaskEmbED LSTMED DCTED PrObe	NaiveDC 12.20% 0.2581 0.8078 0.5946 0.5844 0.6808 0.8911 0.9786 0.9611 0.9452 0.9652 Faa NaiveDC 45.42%	DCT 79.00% 0.5622 0.6382 0.7001 0.6702 0.6550 0.4800 0.3922 0.6352 0.5515 0.5905 ctory Pack DCT 88.75%	SCAN 66.60% 0.5000 0.6193 0.6734 0.5962 0.6759 0.5086 0.4865 0.6356 0.5255 0.6983 ing	NaiveDC 08.89% 0.4621 0.3221 0.4148 0.6022 0.8446 0.9367 0.9375 0.9555 0.9679 0.9903	DCT 29.17% 0.5537 0.7220 0.7707 0.4772 0.7276 0.8652 0.9314 0.9546 0.8534 0.9438 Statistics	SCAN 58.89% 0.5498 0.7041 0.8237 0.7489 0.8614 0.6433 0.7401 0.8913 0.7880 0.9097
AUROC	SVDDED TaskEmbED LSTMED DCTED PrObe SVDDED TaskEmbED LSTMED DCTED PrObe	NaiveDC 12.20% 0.2581 0.8078 0.5946 0.5844 0.6808 0.8911 0.9786 0.9611 0.9452 0.9652	DCT 79.00% 0.5622 0.6382 0.7001 0.6702 0.6550 0.4800 0.3922 0.6352 0.5515 0.5905	SCAN 66.60% 0.5000 0.6193 0.6734 0.5962 0.6759 0.5086 0.4865 0.6356 0.5255 0.6983 ing SCAN 63.75%	NaiveDC 08.89% 0.4621 0.3221 0.4148 0.6022 0.8446 0.9367 0.9375 0.9555 0.9679 0.9903 Top 1 counts	DCT 29.17% 0.5537 0.7220 0.7707 0.4772 0.7276 0.8652 0.9314 0.9546 0.8534 0.9438 Statistics Av	SCAN 58.89% 0.5498 0.7041 0.8237 0.7489 0.8614 0.6433 0.7401 0.8913 0.7880 0.9097
AUROC	SVDDED TaskEmbED LSTMED DCTED PrObe SVDDED TaskEmbED LSTMED DCTED PrObe AED	NaiveDC 12.20% 0.2581 0.8078 0.5946 0.5844 0.6808 0.8911 0.9786 0.9611 0.9452 0.9652 Fac NaiveDC 45.42% 0.3338	DCT 79.00% 0.5622 0.6382 0.7001 0.6702 0.6550 0.4800 0.3922 0.6352 0.5515 0.5905 ettory Pack DCT 88.75% 0.3849	SCAN 66.60% 0.5000 0.6193 0.6734 0.5962 0.6759 0.5086 0.4865 0.6356 0.5255 0.6983 ing SCAN 63.75%	NaiveDC 08.89% 0.4621 0.3221 0.4148 0.6022 0.8446 0.9367 0.9375 0.9555 0.9679 0.9903 Top 1 counts	DCT 29.17% 0.5537 0.7220 0.7707 0.4772 0.7276 0.8652 0.9314 0.9546 0.8534 0.9438 Statistics Av Ra	SCAN 58.89% 0.5498 0.7041 0.8237 0.7489 0.8614 0.6433 0.7401 0.8913 0.7880 0.9097
AUROC AUPRC Metric [†]	SVDDED TaskEmbED LSTMED DCTED PrObe SVDDED TaskEmbED LSTMED DCTED PrObe AED SVDDED TaskEmbED LSTMED DCTED DCTED DCTED DCTED DCTED	NaiveDC 12.20% 0.2581 0.8078 0.5946 0.5844 0.6808 0.8911 0.9786 0.9611 0.9452 0.9652 Fac NaiveDC 45.42% 0.3338 0.5564 0.6471 0.5361	DCT 79.00% 0.5622 0.6382 0.7001 0.6702 0.6550 0.4800 0.3922 0.6352 0.5515 0.5905 ctory Pack DCT 88.75% 0.3849 0.7201 0.7934 0.7509	SCAN 66.60% 0.5000 0.6193 0.6734 0.5962 0.6759 0.5086 0.4865 0.6356 0.5255 0.6983 ing SCAN 63.75% 0.6151 0.6916 0.7836 0.5006	NaiveDC 08.89% 0.4621 0.3221 0.4148 0.6022 0.8446 0.9367 0.9375 0.9555 0.9679 0.9903 Top 1 counts	DCT 29.17% 0.5537 0.7220 0.7707 0.4772 0.7276 0.8652 0.9314 0.9546 0.8534 0.9438 Statistics Av Ra 2	SCAN 58.89% 0.5498 0.7041 0.8237 0.7489 0.8614 0.6433 0.7401 0.8913 0.7880 0.9097 vg. unk .2 .2
AUROC AUPRC Metric [†]	SVDDED TaskEmbED LSTMED DCTED PrObe SVDDED TaskEmbED LSTMED DCTED PrObe AED SVDDED TaskEmbED LSTMED	NaiveDC 12.20% 0.2581 0.8078 0.5946 0.5844 0.6808 0.8911 0.9786 0.9611 0.9452 0.9652 Fac NaiveDC 45.42% 0.3338 0.5564 0.6471	DCT 79.00% 0.5622 0.6382 0.7001 0.6702 0.6550 0.4800 0.3922 0.6352 0.5515 0.5905 ctory Pack DCT 88.75% 0.3849 0.7201 0.7934	SCAN 66.60% 0.5000 0.6193 0.6734 0.5962 0.6759 0.5086 0.4865 0.6356 0.5255 0.6983 ing SCAN 63.75% 0.6151 0.6916 0.7836	NaiveDC 08.89% 0.4621 0.3221 0.4148 0.6022 0.8446 0.9367 0.9375 0.9555 0.9679 0.9903 Top 1 counts	DCT 29.17% 0.5537 0.7220 0.7707 0.4772 0.7276 0.8652 0.9314 0.9546 0.8534 0.9438 Statistics Av Ra 2	SCAN 58.89% 0.5498 0.7041 0.8237 0.7489 0.8614 0.6433 0.7401 0.8913 0.7880 0.9097 vg. unk
AUROC AUPRC Metric [†]	SVDDED TaskEmbED LSTMED DCTED PrObe SVDDED TaskEmbED LSTMED DCTED PrObe AED SVDDED TaskEmbED LSTMED DCTED TaskEmbED LSTMED SVDDED TaskEmbED LSTMED DCTED PrObe SVDDED	NaiveDC 12.20% 0.2581 0.8078 0.5946 0.5844 0.6808 0.8911 0.9786 0.9611 0.9452 0.9652 Fac NaiveDC 45.42% 0.3338 0.5564 0.6471 0.5361 0.6635	DCT 79.00% 0.5622 0.6382 0.7001 0.6702 0.6550 0.4800 0.3922 0.6352 0.5515 0.5905 ctory Pack DCT 88.75% 0.3849 0.7201 0.7509 0.7670	SCAN 66.60% 0.5000 0.6193 0.6734 0.5962 0.6759 0.5086 0.4865 0.6356 0.5255 0.6983 ing SCAN 63.75% 0.6151 0.6916 0.7836 0.5006 0.8256	NaiveDC 08.89% 0.4621 0.3221 0.4148 0.6022 0.8446 0.9367 0.9375 0.9555 0.9679 0.9903 Top 1 counts 1 3 4 0 13 0	DCT 29.17% 0.5537 0.7220 0.7707 0.4772 0.7276 0.8652 0.9314 0.9546 0.8534 0.9438 Statistics Av Ra 4 3 2 3 1 4	SCAN 58.89% 0.5498 0.7041 0.8237 0.7489 0.8614 0.6433 0.7401 0.8913 0.7880 0.9097 vg. unk .2 .2 .8 .2 .5
AUROC AUPRC Metric [↑] AUROC	SVDDED TaskEmbED LSTMED DCTED PrObe SVDDED TaskEmbED LSTMED DCTED PrObe AED SVDDED TaskEmbED LSTMED DCTED TaskEmbED SVDDED TaskEmbED LSTMED DCTED PrObe SVDDED TaskEmbED	NaiveDC 12.20% 0.2581 0.8078 0.5946 0.5844 0.6808 0.8911 0.9786 0.9611 0.9452 0.9652 Fac NaiveDC 45.42% 0.3338 0.5564 0.6471 0.5361 0.6635	DCT 79.00% 0.5622 0.6382 0.7001 0.6702 0.6550 0.4800 0.3922 0.5515 0.5905 ctory Pack DCT 88.75% 0.3849 0.7201 0.7509 0.7670 0.1600 0.5002	SCAN 66.60% 0.5000 0.6193 0.6734 0.5962 0.6759 0.5086 0.4865 0.6356 0.5255 0.6983 ing SCAN 63.75% 0.6151 0.6916 0.7836 0.5006 0.8256 0.5657 0.7287	NaiveDC 08.89% 0.4621 0.3221 0.4148 0.6022 0.8446 0.9367 0.9375 0.9555 0.9679 0.9903 Top 1 counts 1 3 4 0 13 0 3	DCT 29.17% 0.5537 0.7220 0.7707 0.4772 0.7276 0.8652 0.9314 0.9546 0.8534 0.9438 Statistics Av Ra 4 3 2 3 1 4 3	SCAN 58.89% 0.5498 0.7041 0.8237 0.7489 0.8614 0.6433 0.7401 0.8913 0.7880 0.9097 vg. mk .2 .2 .8 .2 .5 .5
AUROC AUPRC Metric [†]	SVDDED TaskEmbED LSTMED DCTED PrObe SVDDED TaskEmbED LSTMED DCTED PrObe AED SVDDED TaskEmbED LSTMED DCTED TaskEmbED LSTMED DCTED TaskEmbED LSTMED DCTED LSTMED DCTED PrObe	NaiveDC 12.20% 0.2581 0.8078 0.5946 0.5844 0.6808 0.8911 0.9786 0.9611 0.9452 0.9652 Fac NaiveDC 45.42% 0.3338 0.5564 0.6471 0.5361 0.6635 0.5583 0.7057 0.7667	DCT 79.00% 0.5622 0.6382 0.7001 0.6702 0.6550 0.4800 0.3922 0.5515 0.5905 ctory Pack DCT 88.75% 0.3849 0.7201 0.7509 0.7670 0.1600 0.5002 0.6335	SCAN 66.60% 0.5000 0.6193 0.6734 0.5962 0.6759 0.5086 0.4865 0.6356 0.5255 0.6983 ing SCAN 63.75% 0.6151 0.6916 0.7836 0.5006 0.8256 0.5657 0.7287 0.8063	NaiveDC 08.89% 0.4621 0.3221 0.4148 0.6022 0.8446 0.9367 0.9375 0.9555 0.9679 0.9903 Top 1 counts 1 3 4 0 13 0 3 3 3	DCT 29.17% 0.5537 0.7220 0.7707 0.4772 0.7276 0.8652 0.9314 0.9546 0.8534 0.9438 Statistics Av Ra 4 3 2 3 1 4 3 2	SCAN 58.89% 0.5498 0.7041 0.8237 0.7489 0.8614 0.6433 0.7401 0.8913 0.7880 0.9097 vg. mk .2 .2 .8 .2 .5 .5
AUROC AUPRC Metric [↑] AUROC	SVDDED TaskEmbED LSTMED DCTED PrObe SVDDED TaskEmbED LSTMED DCTED PrObe AED SVDDED TaskEmbED LSTMED DCTED TaskEmbED SVDDED TaskEmbED LSTMED DCTED PrObe SVDDED TaskEmbED	NaiveDC 12.20% 0.2581 0.8078 0.5946 0.5844 0.6808 0.8911 0.9786 0.9611 0.9452 0.9652 Fac NaiveDC 45.42% 0.3338 0.5564 0.6471 0.5361 0.6635	DCT 79.00% 0.5622 0.6382 0.7001 0.6702 0.6550 0.4800 0.3922 0.5515 0.5905 ctory Pack DCT 88.75% 0.3849 0.7201 0.7509 0.7670 0.1600 0.5002	SCAN 66.60% 0.5000 0.6193 0.6734 0.5962 0.6759 0.5086 0.4865 0.6356 0.5255 0.6983 ing SCAN 63.75% 0.6151 0.6916 0.7836 0.5006 0.8256 0.5657 0.7287	NaiveDC 08.89% 0.4621 0.3221 0.4148 0.6022 0.8446 0.9367 0.9375 0.9555 0.9679 0.9903 Top 1 counts 1 3 4 0 13 0 3	DCT 29.17% 0.5537 0.7220 0.7707 0.4772 0.7276 0.8652 0.9314 0.9546 0.8534 0.9438 Statistics Av Ra 4 3 2 3 1 4 3 2 3 3 1	SCAN 58.89% 0.5498 0.7041 0.8237 0.7489 0.8614 0.6433 0.7401 0.8913 0.7880 0.9097 vg. unk .2 .2 .8 .2 .5 .5

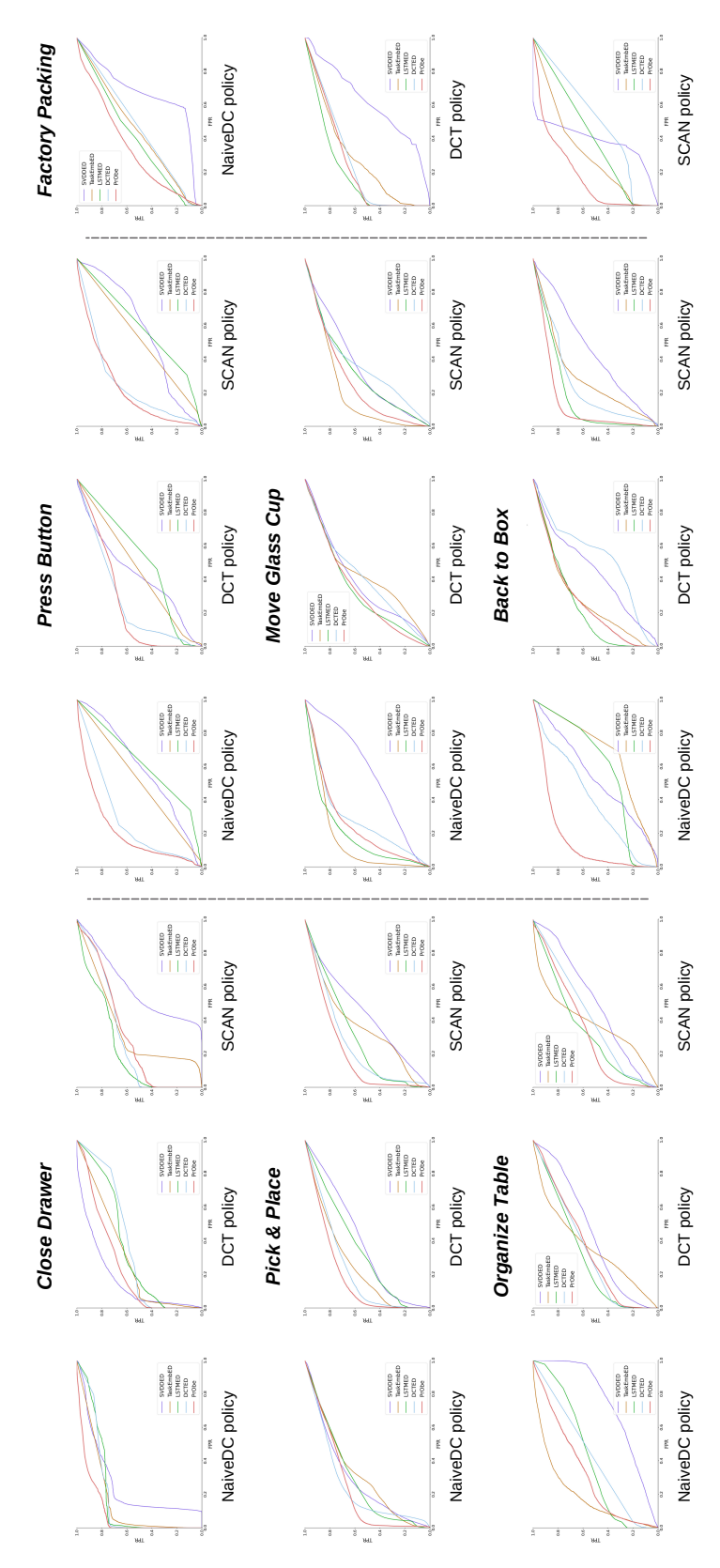


Figure 15. AED methods's ROC curves of all FSI tasks. The AUROC scores reported in Table 8 are the area under the curves.